The MNK - eIF4E signaling axis contributes to injury-induced nociceptive plasticity and the development of chronic pain

Title: The MNK – eIF4E signaling axis contributes to injury-induced nociceptive plasticity and the development of chronic pain

Abbreviated Title: eIF4E phosphorylation controls pain plasticity

Jamie K Moy[1,2], Arkady Khoutorsky[3,9], Marina N Asiedu[1,2], Bryan J Black[5], Jasper L Kuhn[1], Paulino Barragán-Iglesias[1], Salim Megat[1], Michael D Burton[1], Carolina C Burgos-Vega[1,2], Ohannes K Melemedjian[2], Scott Boitano[4,6], Josef Vagner[6], Christos G Gkogkas[7], Joseph J Pancrazio[5], Jeffrey S. Mogil[8], Gregory Dussor[1,2], Nahum Sonenberg[3], Theodore J Price[1,2,*]

[1]School of Behavioral and Brain Sciences, University of Texas at Dallas, Richardson, TX 75080
[2]Department of Pharmacology, University of Arizona, Tucson, AZ 85724
[3]Department of Biochemistry and Goodman Cancer Research Center, McGill University, Montréal, Canada H3A 1A3
[4]Department of Physiology, University of Arizona, Tucson, AZ 85724
[5]Department of Bioengineering, University of Texas at Dallas, Richardson, TX 75080
[6]Bio5 Research Collaborative Institute, University of Arizona, Tucson, AZ 85724
[7]Patrick Wild Centre and Centre for Integrative Physiology, University of Edinburgh, Edinburgh, UK EH8 9XD
[8]Department of Psychology and Alan Edwards Centre for Research on Pain, McGill University, Montréal, Canada H3A 0G1
[9]Department of Anesthesia and Alan Edwards Centre for Research on Pain, McGill University, Montréal, Canada H3A 0G1

[*] Corresponding author
Theodore J Price
School of Behavioral and Brain Sciences
University of Texas at Dallas
JO 4.212
800 W Campbell Rd
Richardson TX 75080
972-883-4311
Theodore.price@utdallas.edu

Number of pages: 38
Number of figures: 12
Number of tables: 3

Number of words for
Abstract: 250
Introduction: 582
Discussion: 1500

The authors declare no competing financial interests.

ACKNOWLEDGEMENTS: This work was supported by NIH grants R01NS065926 (TJP), R01GM102575 (TJP and GD), R01NS073664 (TJP, SB and JV), The University of Texas STARS program (TJP and GD), and the postdoctoral CONACYT fellowship program (PBI).

ABSTRACT

The sensitization of nociceptors generates injury-induced pain states and contributes to the development of chronic pain. Previous studies show that inhibiting mRNA translation through mechanistic target of rapamycin (mTOR) and mitogen activated protein kinase (MAPK) pathways blocks the development of nociceptor sensitization. These pathways signal convergently to the mRNA elongation initiation factor (eIF) 4F complex to regulate sensitization of nociceptors but the details of this process are obscure. Here we investigated the hypothesis that phosphorylation of the 5' cap-binding protein, eIF4E, by its specific kinase MAPK interacting kinase (MNK) 1/2 is a key factor in nociceptor sensitization and the transition to chronic pain using *eIF4E*^{S209A} mice. Phosphorylation of ser209 on eIF4E regulates the translation of a subset of mRNAs. We show that pro-nociceptive and inflammatory factors, such as nerve growth factor (NGF), interleukin 6 (IL-6) and carrageenan, produce decreased mechanical and thermal hypersensitivity, decreased affective pain behaviors and strongly reduced hyperalgesic priming in the absence of eIF4E phosphorylation. Moreover, in patch clamp electrophysiology and Ca^{2+} imaging experiments on dorsal root ganglion (DRG) neurons, the effects of NGF and IL-6 on excitability measures are attenuated in neurons from *eIF4E*^{S209A} mice. These effects were recapitulated in *Mnk1/2*$^{-/-}$ mice and with the MNK1/2 inhibitor, cercosporamide. We also find that cold hypersensitivity induced by peripheral nerve injury is reduced in *eIF4E*^{S209A} and *Mnk1/2*$^{-/-}$ mice and by cercosporamide treatment. Our findings demonstrate that the MNK1/2 – eIF4E signaling axis is a major contributing factor to mechanisms of nociceptor plasticity and the transition to chronic pain.

SIGNIFICANCE STATEMENT

Chronic pain is a debilitating disease affecting approximately 1 in 3 Americans. Chronic pain is thought to be driven by changes in the excitability of peripheral nociceptive neurons but the precise mechanisms controlling these changes are not elucidated. Emerging evidence demonstrates that mRNA translation regulation pathways are key factors in changes in nociceptor excitability. Our work demonstrates that a single phosphorylation site on the 5' cap-binding protein eIF4E is a critical mechanism for changes in nociceptor excitability that drive the development of chronic pain. We reveal a new mechanistic target for the transition to a chronic pain states and propose that targeting the upstream kinase, MNK1/2, could be used as a therapeutic approach for chronic pain.

INTRODUCTION

Translation of mRNAs is dynamically regulated in cells by upstream signaling factors that respond to a broad variety of receptors including ion channels, G-protein coupled receptors (GPCRs) and tyrosine receptor kinases (trks). For example, in DRG neurons nerve growth factor (NGF) and interleukin 6 (IL-6), two extracellular ligands intimately linked to pain across mammalian species, signal via their cognate receptors to the mTOR and MAPK pathways to induce eIF4F complex formation and promote translation (Melemedjian et al., 2010). The eIF4F complex is composed of the 5' cap binding protein eIF4E, the deadbox RNA helicase eIF4A, and the scaffolding protein eIF4G. Phosphorylation of 4E-binding proteins (4E-BPs) by mTOR relieves inhibition on eIF4E and allows for eIF4E association with eIF4G and eIF4A to form the eIF4F complex, which promotes cap-dependent translation (Sonenberg and Hinnebusch, 2009). On the other hand, MAPKs act via the MAPK interacting kinases MNK1/2 to phosphorylate eIF4E at Serine 209 (Pyronnet et al., 1999; Waskiewicz et al., 1999). Interestingly, the precise role of eIF4E phosphorylation is not known but eIF4E phosphorylation has been linked to cellular plasticity in cancer (Furic et al., 2010) and immunity (Herdy et al., 2012). Its physiological role in the context of sensory neuron plasticity leading to pathological pain is unexplored.

The diversity of mechanisms of translation control by the eIF4F proteins is more complex than previously thought. It is now known that specific phosphorylation events on specific eIF4F complex proteins control the translation of specific subsets of mRNAs. The mTOR pathway has recently been shown to primarily influence the translation of mRNAs that contain terminal oligopyrimidine tracts in their 5' untranslated regions (UTRs) (Thoreen et al., 2012). Similarly, the RNA helicase eIF4A primarily influences the translation of mRNAs with highly structured 5' UTRs and/or 5' UTRs that contain sequence motifs that form G quadruplexes (Wolfe et al., 2014). In the context of pain, two recent studies have shown distinct phenotypes in 4E-BP1 knockout mice or when eIF2α phosphorylation is genetically reduced. 4E-BP1 knockout mice show increased spinal cord expression of neuroligin 1 and enhanced mechanical sensitivity with no change in thermal thresholds (Khoutorsky et al., 2015). On the other

hand, mice lacking eIF2α phosphorylation on one allele have reduced responses to thermal stimulation and a deficit in thermal hypersensitivity after inflammation but normal mechanical pain (Khoutorsky et al., 2016). These studies highlight that distinct translation regulation signaling pathways produce diverse sensory phenotypes.

The goal of this study was to test the hypothesis that eIF4E phosphorylation is a central regulator of nociceptive plasticity and the transition to a chronic pain state. We tested this hypothesis using mice lacking the phosphorylation site for MNK1/2 on eIF4E (*eIF4E*^{S209A}), mice lacking both *Mnk1* and *2* (*Mnk*$^{-/-}$) (Ueda et al., 2004) and an inhibitor of MNK1/2 kinase activity, cercosporamide (Altman et al., 2013). We find that, different from 4E-BP1 knockouts or eIF2α mutants (Khoutorsky et al., 2015; Khoutorsky et al., 2016), eIF4E phosphorylation does not influence acute pain behavior but does promote nociceptor sensitization by a variety of endogenous factors known to promote pain in humans (NGF and IL-6) as well as exogenous pain-sensitizing factors. Moreover, eIF4E phosphorylation is a major contributor to the transition to a chronic pain state as shown in hyperalgesic priming, where mechanical hypersensitivity and grimacing is decreased and in neuropathic pain models where cold hypersensitivity is decreased. Our findings elucidate a new pathway regulating plasticity in the nociceptive system with implications for understanding signaling mechanisms in nociceptors that promote the transition to a chronic pain state.

MATERIALS and METHODS

Experimental animals

Male and female *eIF4E*^{S209A} mice on a C57BL/6 background were generated in the Sonenberg laboratory at McGill University, as described previously (Furic et al., 2010), and bred at The University of Arizona or The University of Texas at Dallas to generate experimental animals. *Mnk1/2*$^{-/-}$ mice on a C57BL/6 background were obtained from Rikiro Fukunaga (Ueda et al., 2004) and bred at McGill University. All animals were genotyped using DNA from ear clips taken at the time of weaning and all animals were backcrossed to C57Bl/6 background for at least 10 generations prior to experiments. All electrophysiological experiments using *eIF4E*^{S209A} and WT mice were performed using mice between the ages of 4 and 6 weeks of age at the start of the experiment. Behavioral experiments using *eIF4E*^{S209A} and WT mice were performed using mice between the ages of 8 and 12 weeks, weighing approximately 20 – 25 g. Experiments using ICR mice obtained from Harlan Laboratories (Houston, TX) were performed using mice between 4 to 8 weeks of age, weighing approximately 20 – 25 g at the start of the experiment. All animal procedures were approved by Institutional Animal Care and Use Committees at The University of Arizona, The University of Texas at Dallas or McGill University and were in accordance with International Association for the Study of Pain guidelines.

Antibodies and chemicals

The peripherin and neurofilament 200 (NF200) antibodies used for immunohistochemistry (IHC) were obtained from Sigma Aldrich (St. Louis, MO). Isolectin B_4 (IB_4) conjugated to Alexa-Fluor 568 and secondary Alexa-Fluor antibodies were from Life Technologies (Grand Island, NY). Calcitonin gene-related peptide (CGRP) antibody was purchased from Peninsula Laboratories International, Inc. (San Carlos, CA). Transient receptor potential V1 (TRPV1) antibody was procured from Neuromics (Edina, MN). The phospho- and total- eIF4E, 4EBP1, ERK, and GAPDH antibodies were obtained from Cell Signaling Technology (Danvers, MA). The phospho- eIF4E antibody used for immunohistochemistry (IHC) was purchased from Abcam (Cambridge, UK). (RS)-3,5-

Dihyroxyphenylglycin (DHPG) was purchased from Tocris Bioscience (Ellisville, MO). Cercosporamide was provided as a generous gift from Eli Lilly and Company (Indianapolis, IN) to the Sonenberg laboratory. Mouse nerve growth factor (NGF) was obtained from Millipore (Billierca, MA). Recombinant human or mouse interleukin-6 (IL-6) was purchased from R & D systems (Minneapolis, MN). 2-aminothiazol-4-yl-LIGRL-NH_2 (2at-LIGRL) was synthesized in our laboratory as described previously (Boitano et al., 2011). Prostaglandin E_2 (PGE_2) was purchased from Cayman chemicals (Ann Arbor, MI). β-cyclodextrin (45% weight/volume in H_2O) was purchased from Sigma Aldrich (St. Louis, MO). All other chemicals were attained from ThermoFisher Scientific (Waltham, MA). See Table 1 for additional details on antibodies and chemicals used in this study.

Behavior

Mice were housed on 12-hr light-/dark cycles with lights on at 7:00 AM. Mice had food and water available *ad libitum*. All behavioral experiments were performed between the hours of 9:00 AM and 4:00 PM. Mice were randomized to groups from multiple cages to avoid using mice from experimental groups that were cohabitating. Sample size was estimated by performing a power calculation using G*Power (version 3.1.9.2). With 80% power, an expectation of d = 2.2 effect size in behavioral experiments, and alpha set to 0.05, the sample size required was calculated as n = 5 per group. We therefore sought to have an n = 6 in all behavioral experiments. Standard deviation (set at 0.3) for the power calculation was based on previously published mechanical threshold data. The actual number of animals used in each experiment was based on available animals of the appropriate sex and weight but was at least n = 5 for behavior experiments, with the exception of testing the effects cercosporamide on cold hypersensitivity after SNI where the sample size was determined by amount of available drug and dosing schedule given previous publications (see Table 2). Mice were habituated for 1 hr to clear acrylic behavioral chambers before beginning the experiment. Mechanical paw withdrawal thresholds were measured using the up-down method (Chaplan et al., 1994) with calibrated Von Frey filaments (Stoelting Company, Wood Dale, IL). Thermal latency was measured

using a Hargreaves device ((Hargreaves et al., 1988) IITC Life Science Inc.) with heated glass. Settings of 29°C glass, 20% active laser power, and 20 sec cut-off were used. Facial grimacing was evaluated using the Mouse Grimace Scale (MGS) as described previously (Langford et al., 2010). Nocifensive behavior in the formalin test was defined as licking, biting, or shaking of the affected paw, and was recorded over an observation period of 45 min. For intraplantar (i.pl.) injections, 50 ng NGF, 0.1 ng IL-6, 10 or 20 ng 2at-LIGRL were diluted in 0.9% saline and injected with a volume of 25 µL via a 30 ½ -gauge needle. For intrathecal (i.t.) injections 50 nmol of DHPG were injected in a volume of 5 µL via a 30 ½ -gauge needle (Hylden and Wilcox, 1980). Cercosporamide for local injection was made up in 10% DMSO and 45% β-cyclodextrin in water and injected into the paw 15 min prior NGF, and simultaneously with 2at-LIGRL. Cercosporamide was injected i.t. in a volume of 5 µL at the time of NGF i.pl. injection. Mice of both sexes were used in most experiments and no significant differences between sexes were noted for drug or genotype in any experiments. Sex of mice used in all behavioral experiments is shown in Table 2. The experimenter was blinded to the genotype of the mice and drug condition in all experiments. Behavioral experiments were performed by *JKM, AK, MNA, PBI and SM*.

Immunohistochemistry (IHC)

Animals were anesthetized with isoflurane and euthanized by decapitation and tissues were flash frozen in O.C.T. on dry ice. Spinal cords were pressure ejected using chilled 1X phosphate buffered saline (PBS). Sections of spinal cord (25 µm), DRG (20 µm), and glaborous skin (25 µm) were mounted onto SuperFrost Plus slides (Thermo Fisher Scientific, Waltham, MA) and fixed in ice-cold 10% or 4% (skin) formalin in 1X PBS for 1 or 4 hr (skin) then subsequently washed 3 times for 5 min each in 1X PBS. Slides were then transferred to a solution for permeabilization made of 1X PBS with 0.2% Triton X-100 (Sigma Aldrich). After 30 min, slides were washed 3 times for 5 min each in 1X PBS. Tissues were blocked for at least 2 hr in 1X PBS and 10% heat-inactivated normal goat

serum. Antibodies for CGRP, IB_4, and TRPV1 were applied together and incubated with spinal cord and DRG sections on slides at 4° C overnight. A combination of TRPV1 and p-eIF4E antibodies were applied to glabrous skin sections and incubated at 4° C overnight. DRG slices were also stained with peripherin and NF200. Immunoreactivity was visualized following 1 hr incubation with goat anti-rabbit, goat anti-mouse, and goat anti-guinea pig Alexa-Fluor antibodies at room temperature. All IHC images are representations of samples taken from 3 animals per genotype except for glaborous skin IHC where 2 animals per genotype were used. Images were taken using an Olympus FluoView 1200 confocal microscope. Analysis of images was done using ImageJ Version 1.48 for Apple OSX (National Institutes of Health, Bethesda, MD).

Western blotting

Male mice were used for all Western blotting experiments and were sacrificed by decapitation following anesthesia and tissues were flash frozen on dry ice. Frozen tissues were homogenized in lysis buffer (50 mM Tris pH 7.4, 150 mM NaCl, 1 mM EDTA pH 8.0, and 1% Triton X-100) containing protease and phosphatase inhibitors (Sigma Aldrich), and homogenized using a pestle. *In vitro* studies testing the effects of cercosporamide (Figure 6A) consisted of cultured primary DRG neurons from ~ 20 g mice. Mice were anesthetized with isoflurane and euthanized by decapitation. DRGs were dissected and placed in chilled Hank's Balanced Salt Solution (HBSS, Invitrogen) until processed. DRGs were then digested in 1 mg/mL collagenase A (Roche) for 25 min at 37 °C then subsequently digested in a 1:1 mixture of 1 mg/mL collagenase D and papain (Roche) for 20 min at 37 °C. DRGs were then triturated in a 1:1 mixture of 1 mg/mL trypsin inhibitor (Roche) and bovine serum albumin (BioPharm Laboratories, LLC), then filtered through a 70 µm cell strainer (Corning). Cells were pelleted then resuspended in Dulbecco's Modified Eagle's Medium (DMEM) / F12 + Glutamax (Life Technologies) containing 10% fetal bovine serum (FBS, Life Technologies), 1% penicillin and streptomycin, and 3 µg/ml 5-fluorouridine with 7 µg/ml uridine to inhibit mitosis of non-neuronal cells and distributed evenly in a 6-well plate coated with poly-D lysine (Becton Dickenson

[BD]). DRG neurons were maintained in a 37°C incubator containing 5% CO_2 with a media change every other day. On day 5, DRG neurons were treated as indicated in the results section, and cells were rinsed with chilled 1X PBS and harvested in lysis buffer containing protease and phosphatase inhibitors (Sigma-Aldrich), and then sonicated for 10 sec. To clear debris, samples were centrifuged at 14,000 rpm for 15 min at 4°C. Ten to 15 μg of protein was loaded into each well and separated by a 10% SDS-PAGE gel. Proteins were transferred to a 0.45 PVDF membrane (Millipore, Billierca, MA) at 30V overnight at 4 °C. Subsequently, membranes were blocked with 5% non-fat dry milk (NFDM) in 1X Tris buffer solution containing Tween 20 (TTBS) for 3 hr. Membranes were washed in 1X TTBS 3 times for 5 min each, then incubated with primary antibody overnight at 4 °C. The following day, membranes were washed 3 times in 1X TTBS for 5 min each, then incubated with the corresponding secondary antibody at room temperature for 30 min to 1 hr. Membranes were then washed with 1X TTBS 6 times for 5 min each. Signals were detected using Immobilon Western Chemiluminescent HRP substrate (Millipore). Bands were visualized using film (Kodak; Rochester, NY) or with a Bio-Rad (Hercules, CA) ChemiDoc Touch. Over-exposed or saturated pixels detected by the ChemiDoc Touch were not used in analysis. Membranes were stripped using Restore Western Blot Stripping buffer (Thermo Fisher Scientific), and re-probed with another antibody. Analysis was performed using ImageJ v1.48 (NIH).

Ca^{2+} Imaging

WT and *eIF4E*^{S209A} DRG neurons were dissociated and cultured as described above with the exception that cells were plated on glass-bottom poly-D-lysine coated dishes (MatTEK Incorporation). DRG neurons were maintained in a 37°C incubator containing 5% CO_2 with no media changes.

Ca^{2+} imaging experiments began 48 hr after dissociation. Each dish was loaded with 10 μg/mL of fura-2 AM (Life Technologies) along with IL-6 (50ng/mL) or vehicle in Hank's Buffered Salt Solution (HBSS, Invitrogen) supplemented with 0.25% w/v bovine serum albumin and 2 mM $CaCl_2$, for 1 hr at 37°C. The cells were then changed to bath solution (125 mM NaCl, 5 mM KCl, 10 mM HEPES, 1 M

$CaCl_2$, 1 M $MgCl_2$, and 2 M glucose pH 7.4 adjusted with N-methyl Glucamine and ~ 300 mosM) for 30 min in a volume of 2 mL for esterification. Dishes were then washed with 2 mL of bath solution prior to recordings. Only neurons were used in the analysis and these were defined as cells with 10% or higher ratiometric change in intracellular Ca^{2+} in response to the 50 mM KCl perfusion. Maximum Ca^{2+} release was calculated by comparing ratio value change by time compared to baseline. A change of at least 10% intracellular Ca^{2+} in response to 1 nM PGE_2 or 250 nM capsaicin was used to classify as neuron as responsive to the stimulus. Experiments were conducted using the MetaFluor Fluorescence Ratio Imaging Software on an Olympus TH4-100 apparatus (Olympus).

Extracellular electrophysiology

MEA-based extracellular recording experiments were performed on dissociated mouse DRG neurons between day-in-vitro 11 and 15 using Ti or ITO 60-channel planar microelectrode arrays (Multichannel Systems, Reutlingen, Germany) equipped with hardware/software from Plexon, Inc. Data were acquired at 40 kHz/channel and digitally filtered (0.1 to 7000 Hz bandpass) during acquisition. An additional 4-pole Butterworth bandpass filter (250 Hz to 7500 Hz) was applied to raw, continuous data, enabling detection of single-event extracellular voltage changes (spikes). Spikes were defined by filtered data crossing a 5σ threshold based on root mean square values calculated for each channel. Active channels were defined by template spike detection resulting in average waveform amplitudes of 40 μV or higher during any of the three 1 hour experimental intervals: baseline, IL-6 treatment, and wash. Between each interval, recording was paused for ~ 2 min to allow for manual exchange of culture medium for medium + IL-6 (IL-6 treatment, 50 ng/mL) or fresh culture medium (Wash). Active channel data was exported to NeuroExplorer (Nex Technologies, Madison, AL) for mean spike rate calculations and further analysis. Statistical comparisons of channel activity were carried out using OriginPro software (OriginLab, Northhampton, MA). MEA cultures were maintained at 37 ˚C, 5% CO_2, and 90% humidity throughout all experiments (OKO Labs, Pozzuoli,

Italy). Culture-surface preparation, DRG extraction, dissociation, and cell seeding was carried out as described above.

Patch-clamp Electrophysiology

For culturing DRGs, acutely dissected DRGs were incubated for 15 min in 20 units/ml Papain (Worthington) followed by 15 min in 3 mg/ml Collagenase Type II (Worthington). After trituration through a fire-polished Pasteur pipette, dissociated cells were resuspended in Liebovitz L-15 medium (Life Technologies) supplemented with 10% fetal bovine serum (FBS), 10 mM glucose, 10 mM HEPES and 50 units/ml penicillin/streptomycin and plated on poly-D-lysine and laminin (Sigma) -coated dishes. Cells were allowed to adhere for several hours at room temperature in a humidified chamber and covered with media described above. DRG neurons were treated with 50 ng/ml NGF 18 – 24 hr prior to recordings or with 50ng/ml mouse IL-6 for 1 hr.

Whole cell patch-clamp experiments were performed on isolated mouse DRG neurons within 24 hr of dissociation using a MultiClamp 700B (Axon Instruments, Sunnyvale, CA) patch-clamp amplifier and PClamp 9 acquisition software (Axon Instruments). Recordings were sampled at 2 kHz and filtered at 1 kHz (Digidata 1322A, Axon Instruments). Pipettes (OD: 1.5mm, ID: 0.86mm) were pulled using a P-97 puller (Sutter Instrument, Novato, CA) and heat polished to 1.5-4 MΩ resistance using a microforge (MF-83, Narishige, East Meadow, NY). Series resistance was typically <7 MΩ and was compensated 60-80%. Data were analyzed using Clampfit 10 (Molecular Devices, Sunnyvale, CA) and Origin 8 (OriginLab, Northhampton, MA). All neurons included in the analysis had a resting membrane potential (RMP) -60 mV or lower. The RMP was recorded 1–3 min after achieving whole-cell configuration. In current-clamp mode, action potentials were elicited by injecting slow ramp currents from 0.1 to 0.7 nA with Δ = 0.2 nA over 1 s to mimic slow depolarization. The pipette solution contained (in mM) 140 KCl, 11 EGTA, 2 $MgCl_2$, 10 NaCl, 10 HEPES, 1 $CaCl_2$ pH 7.3 (adjusted with N-methyl glucamine), and was ~ 320 mosM. External solution contained (in mM) 135 NaCl, 2 $CaCl_2$, 1 $MgCl_2$, 5 KCl, 10 Glucose, 10 HEPES, pH 7.4 (adjusted with N-methyl glucamine), and was ~ 320

mosM. For neuronal VGNaC current recordings, pipette solution contained (in mM) 120 CsCl, 10 EGTA, 2 $MgCl_2$, 5 NaCl, 10 HEPES, 2 $CaCl_2$, pH 7.3 (adjusted with N-methyl glucamine) and osmolarity was 320 mosM. External solution contained (in mM) 95 Choline, 20 Tetraethyl ammonium (TEA), 20 NaCl, 2 $CaCl_2$, 1 $MgCl_2$, 10 HEPES, 5 KCl, 0.1 $CdCl_2$, 0.1 $NiCl_2$, pH 7.3 (adjusted with N-methyl glucamine) and osmolarity was 320 mosM. In whole-cell configuration, cells were voltage-clamped and VGNaC currents were evoked by a 50 ms depolarizing steps (from -80 to +40 mV in 5 mV increments) from a holding potential of -120mV. Sodium currents were normalized to whole-cell capacitance and expressed as current density (pA/pF).

Statistics

All data are represented as mean ± standard error of the mean (SEM). Individual data points are represented in each graph to show the n in each group and the overall distribution of individual data points. All analysis was done using GraphPad Prism 6 v 6.0 for Mac OS X. Single comparisons were performed using Student's *t*-test and multiple comparisons were performed using a two-way ANOVA with Bonferroni posthoc tests for across group comparisons or Uncorrected Fisher's LSD for within group comparisons. Raw data from all experiments, including all of the statistical analysis, is available in prism file format as extended data.

RESULTS

Nociceptive reflexes, acute pain behavior and development of DRG to spinal dorsal horn connectivity is normal in eIF4E^{S209A} mice

To test the hypothesis that eIF4E phosphorylation is a key factor in pain sensitization and the transition to a chronic pain state we used mice harboring a point mutation on the only known phosphorylation site in the eIF4E protein, S209 (Furic et al., 2010; Herdy et al., 2012; Gkogkas et al., 2014). We compared baseline thermal (Figure 1A) and mechanical thresholds (Figure 1B) between *eIF4E^{S209A}* mice and their wildtype (WT) littermates and noted no differences in tail flick latencies to 55°C water or von Frey stimulation. When 5% formalin, a commonly used noxious irritant, was injected into the hindpaw no differences in pain behaviors were noted between genotypes in either the first (Figure 1C, 0 – 10 min) or second (Figure 1D, 15 – 45 min) phases of the test. However, when mechanical sensitivity was examined 3 days after formalin administration there was a striking difference between genotypes, with *eIF4E^{S209A}* mice failing to develop mechanical hypersensitivity. The group I metabotropic glutamate receptor (mGluR) agonist, dihydroyphenylglycine (DHPG), promotes tonic pain-related behaviors when injected intrathecally (Karim et al., 2001). These behaviors are decreased by inhibition of spinal mTOR signaling (Price et al., 2007). We did not detect any difference in acute pain behaviors upon DHPG intrathecal (i.t.) injection between genotypes (Figure 1F), but 6 hr following injection *eIF4E^{S209A}* mice again showed a reduction in the magnitude of mechanical hypersensitivity (Figure 1G).

We next used a variety of histochemical markers to assess the possibility of developmental differences in sensory anatomy between *eIF4E^{S209A}* mice and WT littermates. In both WT (Figure 2A) and *eIF4E^{S209A}* (Figure 2B) mice there was a clear delineation between the projections of calcitonin gene-related peptide (CGRP) positive afferents and the isolectin B_4 (IB_4) population to lamina II of the dorsal horn. This was also true for TRPV1-positive and IB_4-positive staining while CGRP and TRPV1 afferents overlapped heavily in projections to lamina I and lamina II. Peripherin is expressed predominately in unmyelinated neurons in the DRG, whereas NF200 staining is used to label

myelinated, large diameter afferents that are mostly Aβ fibers. These two populations were non-overlapping in both genotypes (Figure 2C) and the proportions of DRG neurons expressing these markers were equivalent (Figure 2C). Neuronal populations expressing TRPV1, IB_4, and CGRP were also no different in *eIF4E*^{S209A} versus WT DRGs (Figure 2D).

We were concerned about the possibility of feedback signaling that might change activity in upstream signaling pathways (Carracedo et al., 2008; Melemedjian et al., 2013) and complicate interpretation of experimental results. We dissected lumbar DRG and dorsal horn of the spinal cord from WT and *eIF4E*^{S209A} mice and examined eIF4E, extracellular signal regulated protein kinase (ERK) and 4E-BP phosphorylation in both tissues by Western blot. While eIF4E phosphorylation was completely absent in *eIF4E*^{S209A} mice, there was no change in either ERK (Figure 3A) or 4E-BP (Figure 3B) phosphorylation in DRG or spinal cord (Figure 3C and D) in *eIF4E*^{S209A} mice. These results rule out the possibility of feedback signaling in the ERK and mTOR pathways in tissues relevant to algesiometric assays.

Deficits in mechanical sensitization, affective pain expression, and the development of hyperalgesic priming in eIF4E^{S209A} *mice*

Previous studies have shown that IL-6, NGF (Melemedjian et al., 2010) and activation of protease activated receptor 2 (PAR2) (Tillu et al., 2015) promote mechanical hypersensitivity in an ERK-dependent fashion that requires *de novo*, local protein synthesis. To test the role of eIF4E phosphorylation in this process we injected IL-6, NGF and the PAR2 agonist, 2at-LIGRL (Flynn et al., 2011) into the hindpaw of WT and *eIF4E*^{S209A} mice. IL-6 (0.1 ng) injected into the paw evoked mechanical hypersensitivity lasting approximately 72 hr (Figure 4A) in WT mice. The magnitude of mechanical hypersensitivity was significantly reduced in *eIF4E*^{S209A} mice 24, 48 and 72 hr after injection (Figure 4A). We, and others, have previously shown that activity-dependent translation regulation pathways are required for the full expression of hyperalgesic priming (Melemedjian et al., 2010; Asiedu et al., 2011; Bogen et al., 2012; Melemedjian et al., 2014; Ferrari et al., 2015a; Ferrari et al., 2015b) but the role of eIF4E phosphorylation in this transition to a chronic pain state has not been addressed.

We “primed” WT and *eIF4E*^{S209A} mice with IL-6 (Figure 4A) and, after their mechanical thresholds had completely returned to baseline, challenged these mice with a dose of PGE_2 (100 ng) that fails to induce mechanical hypersensitivity in “unprimed” mice. We observed that the response to PGE_2 injection in *eIF4E*^{S209A} mice was blunted compared to WT mice (Figure 4B).

Similar experiments were done using a hindpaw injection of NGF (50 ng). NGF evoked robust mechanical hypersensitivity in WT mice, whereas in *eIF4E*^{S209A} mice it was dramatically reduced (Figure 5C). After the mice returned to baseline mechanical thresholds, we assessed priming with a hindpaw injection of PGE_2. We observed that similar to IL-6-induced priming, NGF was unable to produce the same magnitude of priming in *eIF4E*^{S209A} mice compared to WT mice (Figure 4D). To examine whether changes in thermal hypersensitivity were also present in these mice we used the Hargreaves test (Hargreaves et al., 1988) in mice treated with NGF. We observed decreased thermal hyperalgesia in *eIF4E*^{S209A} mice compared to WT (Figure 4E) and a transient thermal hypersensitivity during priming in WT mice, but no change in *eIF4E*^{S209A} mice (Figure 4F).

Likewise, the specific PAR2 agonist 2at-LIGRL (20 ng) evoked mechanical hypersensitivity and hyperalgesic priming precipitated by PGE_2 in WT mice but this effect was strongly reduced in *eIF4E*^{S209A} mice (Figure 4G and H). These results indicate that eIF4E phosphorylation is a key downstream event for pronociceptive factors that act via the ERK pathway to promote mechanical and thermal hypersensitivity, but whether this also influences spontaneous, non-evoked components of pain is not known. We used the mouse grimace scale (MGS) (Langford et al., 2010) to determine this with hindpaw injection of 2at-LIGRL (20 ng). While PAR2 activation induced a robust grimacing in WT mice, this effect was reduced in *eIF4E*^{S209A} mice (Figure 4I) suggesting that this signaling pathway is critical for full expression of affective pain components downstream of ERK activation. Additionally, when we measured facial grimacing in response to PGE_2 injection in mice previously injected with 2at-LIGRL, there was a significant increase in grimacing in WT mice but no change in facial expression scores in eIF4E^{S209A} mice (Figure 4J).

Mechanical and thermal hypersensitivity induced by complex inflammatory stimuli are regulated by MNK1/2- eIF4E phosphorylation signaling

While the findings above indicate that eIF4E phosphorylation strongly contributes to mechanical and thermal hypersensitivity induced by algogens that signal via ERK, we asked if eIF4E phosphorylation likewise play an important role in mechanical and thermal hypersensitivity induced by inflammation. We utilized a hindpaw injection of carrageenan (0.5% w/v) in WT and *eIF4E*^{S209A} mice and measured mechanical (Figure 5A) and thermal hypersensitivity (Figure 5B). WT mice developed robust mechanical and thermal hypersensitivity whereas this effect was abrogated in *eIF4E*^{S209A} mice (Figure 5A and B). When we tested if carrageenan-induced hyperalgesic priming was dependent on eIF4E phosphorylation, we observed that WT mice developed increased long-lasting mechanical hypersensitivity compared to *eIF4E*^{S209A} mice when priming was precipitated with PGE_2 injection (Figure 5C).

Additionally, we utilized mice lacking *MNK1* and *2 (MNK*$^{-/-}$ *mice)* and complete Freund's adjuvant (CFA) to further test the role of this signaling axis in inflammatory pain. We injected CFA (0.5 mg/mL in 10µL) into the hindpaw of WT and *MNK*$^{-/-}$ mice. While we observed mechanical (Figure 5D) and thermal (Figure 5E) hypersensitivity in both WT and *MNK*$^{-/-}$ mice at early time points, *MNK*$^{-/-}$ mice recovered faster than their WT littermates. When we tested if *MNK*$^{-/-}$ mice transitioned into the "primed" state with a subsequent injection of PGE_2, we saw reduced mechanical (Figure 5F) and thermal (Figure 5G) hypersensitivity in *MNK*$^{-/-}$ mice but a robust response in WT mice.

Pharmacological inhibition of MNK1/2 with cercosporamide recapitulates eIF4E^{S209A} *phenotypes*

To determine whether cercosporamide inhibits eIF4E phosphorylation in DRG neurons these cells were cultured for 5 days and exposed to 10 µM cercosporamide (Altman et al., 2013) or vehicle for 1 hr. Western blot analysis demonstrated a significant decrease of p-eIF4E in treated DRG neurons compared to vehicle (Figure 6A). Cercosporamide-treated DRG neurons showed no change in levels of p-4E-BP1 (Figure 6B), indicating that cercosporamide does not induce feedback activation of mTORC1. Levels of p-ERK were also unchanged (Figure 6C), demonstrating that upstream regulators

of MNK1/2 are unaffected by cercosporamide, and are not activated via a feedback mechanism as we have shown previously for mTORC1 inhibitors (Melemedjian et al., 2013). We also assessed whether systemic injection of cercosporamide (40 mg/kg) (Gkogkas et al., 2014)) in mice influenced eIF4E phosphorylation. In DRG tissue taken 2 hr after cercosporamide injection we observed a ~50% decrease in eIF4E phosphorylation (Figure 6D), whereas no effect was observed in 4E-BP1 phosphorylation (Figure 6E).

We then determined the effects of cercosporamide on NGF- and PAR2 activation-induced mechanical hypersensitivity and hyperalgesic priming *in vivo*. Similar to observations in *eIF4E*^{S209A} mice, treatment with cercosporamide (10 μg, intraplantar) 15 min prior to NGF (Figure 6F) produced blunted mechanical hypersensitivity acutely. Similar results were obtained when 2at-LIGRL was applied in the presence or absence of cercosporamide (Figure 6G). When animals treated with NGF or 2at-LIGRL were subsequently tested for hyperalgesic priming with PGE_2 (Figure 6H and I) there was also a reduction in the magnitude of mechanical hypersensitivity. Moreover, co-injection of cercosporamide with 2at-LIGRL attenuated grimacing recorded 3 hr after injection (Figure 6J), and prevented facial grimacing (Figure 6K) in response to PGE_2 injection, again consistent with observations in *eIF4E*^{S209A} mice.

Our demonstration that hindpaw cercosporamide administration reduces behavioral pain plasticity suggests that p-eIF4E-mediated local translation in peripheral nociceptive fibers contributes to this effect. We therefore sought to evaluate whether p-eIF4E could be observed in nerve fibers innervating the hindpaw. Glabrous skin from both WT and *eIF4E*^{S209A} mice was immunostained for TRPV1 and p-eIF4E and imaged. We observed p-eIF4E in TRPV1 positive nerve fibers in WT mice and this staining was completely absent in *eIF4E*^{S209A} mouse skin samples (Figure 6L) demonstrating the specificity of this antibody and the presence of p-eIF4E in terminals of TRPV1-positive nociceptors.

eIF4E phosphorylation regulates DRG neuron excitability following NGF and IL-6 exposure

To directly test the effect of NGF and IL-6 on DRG neuron excitability in the presence and absence of eIF4E phosphorylation we used patch clamp electrophysiology. DRG neurons were isolated

from WT and *eIF4E*^{S209A} mice and exposed to 50 ng/mL NGF or vehicle for 18 – 24 hr prior to recordings. In WT neurons, NGF caused an increase in the number of action potentials fired in response to slowly depolarizing ramp currents of 100 through 700 pA amplitudes (Figure 7A). In contrast, DRG neurons isolated from *eIF4E*^{S209A} mice showed elevated baseline excitability versus WT neurons but did not show a change in their excitability after exposure to the same concentration of NGF over an identical time course (Figure 7B). For the DRG neurons sampled from both treatments and genotypes there were no differences in membrane capacitance (Figure 7C) or other parameters such as resting membrane potential (WT: -63.34 ± 1.12 mV, n=10; *eIF4E*^{S209A}: -61.63 ± 1.13 mV, n =11, $p < 0.05$, t-test). We next examined NGF-induced changes in DRG excitability in the presence of cercosporamide (10 μM) for 1 hr prior to recordings. Analogous to *eIF4E*^{S209A} DRG neurons, cercosporamide inhibited NGF-induced hyperexcitability (Figure 7D), demonstrating that brief pharmacological inhibition of MNK1/2 reverses augmented excitability in DRG neurons induced by NGF treatment.

Similar experiments were conducted with IL-6 (50 ng/mL), except that IL-6 was only applied for 1 hr prior to patch clamp recordings. IL-6, as we have observed previously in rat trigeminal ganglion neurons (Yan et al., 2012), caused an increase in the number of action potentials fired in response to ramp current injection at 300, 500 and 700 pA amplitudes (Figure 7E). As we observed with NGF, IL-6 failed to increase the excitability of DRG neurons from *eIF4E*^{S209A} mice (Figure 7F). Again, there were no significant differences in membrane capacitance in the populations sampled for any of these experimental conditions (Figure 7G). When we examined the effect of cercosporamide on IL-6-induced hyperexcitability, we found that synonymous to *eIF4E*^{S209A} DRG neurons, cercosporamide inhibited increased neuronal excitability induced by IL-6 treatment (Figure 7H).

To assess if cercosporamide is specific to MNK1/2 in our behavioral paradigm, we utilized cercosporamide in *eIF4E*^{S209A} mice and measured mechanical hypersensitivity induced by NGF. We found no differences in NGF-induced mechanical hypersensitivity between cercosporamide and vehicle injected *eIF4E*^{S209A} mice (Figure 8A). Subsequent injection of PGE_2 to precipitate hyperalgesic priming, additionally showed no difference in either *eIF4E*^{S209A} mice previously injected with cercosporamide or

vehicle (Figure 8B). While these behavioral results suggest that cercosporamide's actions are specific to MNK1/2, we also tested for a possible acute effect of cercosporamide on voltage-gated sodium channels (VGNaC) that could lead to a decrease in excitability and confound results with this drug. VGNaC currents were elicited in cultured DRG neurons by 50 msec depolarizing steps and currents were expressed as current density. Acute application of cercosporamide (10μM) had no effect on VGNaC density ruling out this possibility (Figure 8C and D).

As an independent assay to support our whole cell patch clamp electrophysiological findings, we assessed excitability with extracellular recordings using microelectrode arrays (MEAs). DRG neurons from both WT and *eIF4E*^{S209A} mice were dissociated and cultured on MEA devices (Breckenridge et al., 1995; Potter and DeMarse, 2001; Frega et al., 2012; Enright et al., 2016) (Figure 9A) for 11 – 15 days prior to recordings. Action potentials were recorded for 1 hr prior to IL-6 exposure, during 1 hr of IL-6 (50ng/mL) treatment, and again during a 1 hr washout period. WT and *eIF4E*^{S209A} neurons were mostly silent during recordings preceding IL-6 exposure. In WT DRG neurons, spiking was significantly increased during IL-6 treatment and was maintained during washout (Figure 9B). In contrast, DRG neurons isolated from *eIF4E*^{S209A} mice, showed a brief increase in spiking in response to IL-6 that rapidly decreased to spiking rates that were significantly less than what was observed in WT neurons (Figure 9C).

The whole cell patch clamp and MEA experiments described above indicate that NGF and IL-6 increase excitability in WT neurons but this response is blunted in *eIF4E*^{S209A} DRG neurons. To further investigate the cellular mechanisms responsible for this effect, we examined the effect of IL-6 treatment on sodium current density. In DRG neurons from WT, there was a significant increase in sodium current density after 1 hr IL-6 treatment compared to vehicle suggesting that IL-6 treatment altered the number of available VGNaCs or changed channel gating properties in WT DRG neurons (Figure 9D). Consistent with voltage ramp experiments, baseline VGNaC density was higher in eIF4E^{S209A} neurons. However, these neurons failed to respond to IL-6 with an increase in VGNaC density (Figure 9E). In fact, we observed a trend toward decreased VGNaC density in *eIF4E*^{S209A} mice. From these experiments we

conclude that while baseline excitability and VGNaC availability may be higher in *eIF4E*^{S209A} nociceptors, these neurons fail to respond to algogens with an increase in VGNaC-mediated responses. Importantly, this baseline increased VGNaC availability in *eIF4E*^{S209A} DRG neurons does not lead to ectopic activity since no difference in spiking was observed at baseline in our MEA experiments (Figure 9B and C) and it does not seem to be recapitulated by brief cercosporamide treatment because we did not observe enhanced excitability in whole cell patch clamp experiments with this drug (Figure 8C and D).

eIF4E phosphorylation regulates IL-6-induced enhancements in Ca^{2+} signaling in DRG neurons

To further elucidate the role of eIF4E phosphorylation on DRG excitability, we investigated IL-6-induced changes in Ca^{2+} signaling in DRG neurons by measuring intracellular Ca^{2+} concentration $[Ca^{2+}]_i$ with ratiometric imaging. Dissociated DRG neurons from both WT (Figure 10A) and *eIF4E*^{S209A} (Figure 10B) mice were loaded with fura-2 and treated with either vehicle or IL-6 (50 ng/mL) for 1 hr. Kinetic changes in $[Ca^{2+}]_i$ in response to PGE_2 (1 nM) were measured in all conditions. WT DRG neurons treated with IL-6 displayed a significant decrease in the latency to peak $[Ca^{2+}]_i$ in response to PGE_2 compared to vehicle-treated neurons (Figure 10C). In contrast, DRG neurons isolated from *eIF4E*^{S209A} mice showed no differences in the kinetics of PGE_2-induced responses between IL-6 and vehicle treatments (Figure 10C). On the other hand, the number of WT DRG neurons responding with a $[Ca^{2+}]_i$ rise above a threshold of 10% was drastically increased after IL-6 treatment whereas no change was observed in *eIF4E*^{S209A} DRG neurons (Figure 10D). Capsaicin-evoked changes in $[Ca^{2+}]_i$ were equivalent in both WT and *eIF4E*^{S209A} DRG neurons (Figure 11A) and the proportion of TRPV1-positive DRG neurons (defined as those neurons responding to the specific agonist capsaicin) was the same in all conditions (Figure 11B), consistent with our immunostaining results. Responses in $[Ca^{2+}]_i$ evoked by increasing extracellular K^+ from 5 mM to 50 mM were also not different between genotypes (Figure 11C).

Cold hypersensitivity after peripheral nerve injury is reduced in eIF4E^{S209A} *and Mnk*$^{-/-}$ *mice*

WT, *Mnk*$^{-/-}$ and *eIF4E*^{S209A} mice were subjected to spared nerve injury (SNI) surgery and mechanical and cold hypersensitivity were measured over the ensuing 35 days. We observed a delay in the development of full mechanical hypersensitivity in *eIF4E*^{S209A} mice but by 14 days these mice developed similar mechanical hypersensitivity to their WT littermates (Figure 12A). On the other hand, in *Mnk*$^{-/-}$ mice mechanical hypersensitivity after SNI was blunted in magnitude compared to WT mice (Figure 12B). *eIF4E*^{S209A} mice displayed significantly less cold hypersensitivity than WT littermates throughout the time course of the experiment (Figure 12C), an effect that was also observed in *Mnk*$^{-/-}$ mice (Figure 12D). Finally, we asked if pharmacological inhibition of MNK1/2 with cercosporamide could alleviate cold hypersensitivity in SNI mice. We waited until 4 weeks after SNI (28 days) when mice display very stable cold hypersensitivity and treated mice with vehicle or 40 mg/kg cercosporamide for 3 consecutive days. On the third day we measured cold sensitivity using the acetone test. We observed decreased cold hypersensitivity in the cercosporamide-treated group at 1 hr after the third injection of drug (Figure 12E), suggesting that even late after the development of neuropathic pain targeting MNK1/2 signaling to eIF4E is able to alleviate some aspects of neuropathic pain.

DISCUSSION

The activity-dependent regulation of protein synthesis is a core mechanism mediating neuronal plasticity (Costa-Mattioli et al., 2009). In the nociceptive system, translation regulation pathways have been shown to contribute to the development and maintenance of pain hypersensitivity in a variety of preclinical models, suggesting that targeting these pathways may lead to new pain therapeutics (Price and Geranton, 2009; Obara et al., 2012; Melemedjian and Khoutorsky, 2015; Price and Inyang, 2015). Here we report that phosphorylation of eIF4E at S209 is a key biochemical event for the sensitization of DRG neurons by pro-nociceptive factors that are known to promote pain in rodents and humans, and that loss of this phosphorylation event does not affect baseline pain behaviors or neurodevelopment in the nociceptive system. Our electrophysiological and Ca^{2+} imaging experiments show that the generation of nociceptor hyperexcitability is influenced by eIF4E phosphorylation by MNK1/2. Moreover, eIF4E phosphorylation plays a key role in the transition to a chronic pain state as reflected by deficiencies in peripherally-mediated hyperalgesic priming and a loss of cold hypersensitivity after peripheral nerve injury. Our genetic and pharmacological experiments demonstrate that targeting MNK1/2 recapitulates the phenotype of *eIF4E*^{S209A} mice pointing out that MNK1/2 might be advantageously targeted in the peripheral nervous system for the treatment and/or prevention of chronic pain conditions.

While upstream signaling factors like mTOR and MAPK have been implicated in pain plasticity using pharmacological tools and biochemical measures (Aley et al., 2001; Zhuang et al., 2004; Price et al., 2007; Jimenez-Diaz et al., 2008; Asante et al., 2009; Codeluppi et al., 2009; Geranton et al., 2009; Asante et al., 2010; Melemedjian et al., 2010; Melemedjian et al., 2011; Obara et al., 2011; Ferrari et al., 2013; Melemedjian et al., 2014), specific downstream mechanisms and mRNA targets linked to these kinase signaling cascades have been elusive until very recently. Recent evidence suggests that different translation regulation targets play strikingly uniquely roles in different aspects of pain sensitivity. For example, genetic loss of a major downstream target of mTORC1, 4E-BP1, leads solely to changes in mechanical sensitivity via central mechanisms governed by a synaptic adhesion molecule

known as neuroligin 1 (Khoutorsky et al., 2015). In contrast, mice lacking a key phosphorylation site for eIF2α on a single allele have deficits in baseline thermal nociception without any changes in mechanical thresholds (Khoutorsky et al., 2016). This phenotype can be recapitulated with pharmacological modulation of eIF2α and a deficit in thermal, but not mechanical, hyperalgesia is also associated with this pathway in inflammatory pain. Collectively, these studies suggest that individual translation regulation pathways may target specific subsets of genes that have profound impacts on certain aspects of nociception (e.g. thermal versus mechanical pain; see Table 3 for a summary of previous findings compared to the present paper). We previously showed that NGF and IL-6 are capable of promoting eIF4E phosphorylation in nociceptors *in vitro*, and that disrupting eIF4F complex formation with 4EGI-1 leads to a blockade of the development of mechanical hypersensitivity and hyperalgesic priming by these pro-nociceptive factors (Melemedjian et al., 2010; Tillu et al., 2015). Here we used *eIF4E*^{S209A} and *MNK*$^{-/-}$ mice and pharmacological tools to definitively demonstrate that eIF4E phosphorylation is a core biochemical event modulating how inflammatory stimuli promote mechanical and thermal hypersensitivity, spontaneous pain responses, and the transition to a chronic pain state. These findings distinguish the MNK1/2 – eIF4E signaling cascade from 4E-BP1 and eIF2α signaling which have specific effects on certain pain modalities. Our results support the conclusion that MNK1/2 – eIF4E signaling plays an important role in altering the excitability of a wide population of nociceptors because genetic and pharmacological manipulation of this pathway had robust effects on thermal and mechanical hypersensitivity, as well as spontaneous pain. In our view, this identifies MNK1/2-mediated eIF4E phosphorylation as a crucial target for plasticity in nociceptors that drives the transition to a chronic pain state. MNK1/2-dependent signaling to eIF4E therefore represents a strong mechanistic target for pharmacological manipulation of chronic pain.

Cold hypersensitivity induced by peripheral nerve injury was decreased in *eIF4E*^{S209A} mice, but mechanical hypersensitivity developed normally, albeit with a delay to reach its full magnitude. This is in contrast to a clear deficit in mechanical hypersensitivity induced by inflammation or common

inflammatory mediators. A potential explanation is that mechanisms involved in changes in mechanical reflex withdrawal responses after peripheral nerve injury are dependent on centrally mediated effects, for instance downregulation of KCC2 function (Coull et al., 2003; Price and Prescott, 2015). This would suggest that different subsets of peripheral afferents are responsible for mechanical hypersensitivity under different injury conditions. In fact, mechanical hypersensitivity following nerve injury persists even when the vast majority of C-fibers are eliminated (Abrahamsen et al., 2008; Minett et al., 2014). On the other hand, eliminating neurons in the TRPM8 lineage is sufficient to eliminate cold hypersensitivity after peripheral nerve injury (Knowlton et al., 2013). We observed a strong decrease in cold hypersensitivity induced by nerve injury in *eIF4E*^{S209A} and *Mnk*$^{-/-}$ mice and cercosporamide treatment was able to lead to a transient decrease in cold hypersensitivity. Therefore, our findings are consistent with the notion that MNK – eIF4E signaling is a key signaling hub for the sensitization of peripheral nociceptive neurons but that this signaling pathway is dispensable for the generation of mechanical hypersensitivity after nerve injury. In the nerve injury scenario this mechanical hypersensitivity could be generated exclusively via Aβ-fiber input coupled to spinal dorsal horn disinhibitory mechanisms such as those observed after spinal BDNF (Lee and Prescott, 2015), cytokine (Kawasaki et al., 2008), chemokine (Gosselin et al., 2005) or PGE_2 (Ahmadi et al., 2002) application or with traumatic injury to peripheral nerves (Coull et al., 2005; Abrahamsen et al., 2008; Minett et al., 2014). Another possibility is that different translation regulation mechanisms are involved in mechanical hypersensitivity after nerve injury. Interestingly, AMP activated protein kinase (AMPK) activators reduce neuropathic mechanical hypersensitivity in rats and mice (Melemedjian et al., 2010). AMPK activation inhibits both mTOR and MAPK pathway signaling (Melemedjian et al., 2010). Therefore, only influencing an end point of MAPK signaling in reduction of eIF4E phosphorylation may be insufficient to reduce neuropathic mechanical hypersensitivity and additional inhibition of mTOR signaling may be needed.

Despite intact normal acute pain behavior and anatomy in *eIF4E*^{S209A} mice we observed that DRG neurons surprisingly trended toward higher levels of excitability in response to slowly depolarizing ramp currents and a larger baseline sodium current density. On the other hand, these neurons fail to

demonstrate a change in excitability in response to either IL-6 or NGF *in vitro*, an effect that is reflected in a behavioral deficit *in vivo*. A very recent study revealed that eIF4E phosphorylation is mechanistically linked to stress granule formation and mRNA sequestration through an interaction with the eIF4E-interacting protein 4E-T and that this leads to suppression of translation of some mRNAs (Martinez et al., 2015). While this has not been explored in neurons, it is possible that eIF4E phosphorylation can suppress translation of certain mRNA species under some circumstances and promote the translation of the same, or other, mRNAs in different circumstances, for instance in response to inflammatory mediators in DRG nociceptors. Such a mechanism linked to eIF4E phosphorylation could lead to the cellular phenotype of increased basal excitability but a loss of induced hyperexcitability in the complete absence of eIF4E phosphorylation. In fact, similar phenotypes have been consistently observed in *Fmr1* knockout mice (a model of fragile X syndrome) leading to baseline alterations in neuronal excitability or in signaling pathway efficacy coupled with a lack of plasticity (Grossman et al., 2006; Hanson and Madison, 2007; Pfeiffer and Huber, 2007; Bureau et al., 2008) including in the nociceptive system (Price et al., 2007). Interestingly, recent studies found that eIF4E phosphorylation is enhanced in fragile X syndrome and that crossing mice lacking fragile X mental retardation protein with *eIF4E*^{S209A} mice or treating *Fmr1* mutant mice with cercosporamide rescues many phenotypes in these mice (Gkogkas et al., 2014).

An unanswered question arising from this work is what are the key mRNA targets for eIF4E phosphorylation in the context of nociceptor excitability. Our electrophysiology and Ca^{2+} imaging experiments provide some possible clues. The trafficking of channels to the membrane is an important regulatory mechanism for nociceptor excitability (Matsuoka et al., 2007; Hudmon et al., 2008; Andres et al., 2013). Our findings are consistent with a model where eIF4E phosphorylation enhances the translation of a subset of mRNAs that influence the membrane trafficking of voltage gated channels (e.g., VGNaCs, consistent with our current density experiments) and G-protein coupled receptors (e.g., PGE_2 receptors, consistent with our Ca^{2+} imaging experiments) to enhance nociceptor excitability and increase their responsiveness to inflammatory mediators. While we cannot currently pinpoint the

identity of these locally translated mRNAs, we have now identified a precise signaling event that can be manipulated to identify these mRNAs. Discovering these eIF4E-controlled mRNAs will yield significant insight into how nociceptors alter their excitability downstream of initial phosphorylation events that are likely more transient than the synthesis of new proteins that contribute to the maintenance of long-term nociceptor plasticity.

REFERENCES CITED

Abrahamsen B, Zhao J, Asante CO, Cendan CM, Marsh S, Martinez-Barbera JP, Nassar MA, Dickenson AH, Wood JN (2008) The cell and molecular basis of mechanical, cold, and inflammatory pain. Science 321:702-705.

Ahmadi S, Lippross S, Neuhuber WL, Zeilhofer HU (2002) PGE(2) selectively blocks inhibitory glycinergic neurotransmission onto rat superficial dorsal horn neurons. Nat Neurosci 5:34-40.

Aley KO, Martin A, McMahon T, Mok J, Levine JD, Messing RO (2001) Nociceptor sensitization by extracellular signal-regulated kinases. J Neurosci 21:6933-6939.

Altman JK, Szilard A, Konicek BW, Iversen PW, Kroczynska B, Glaser H, Sassano A, Vakana E, Graff JR, Platanias LC (2013) Inhibition of Mnk kinase activity by cercosporamide and suppressive effects on acute myeloid leukemia precursors. Blood 121:3675-3681.

Andres C, Hasenauer J, Ahn HS, Joseph EK, Isensee J, Theis FJ, Allgower F, Levine JD, Dib-Hajj SD, Waxman SG, Hucho T (2013) Wound-healing growth factor, basic FGF, induces Erk1/2-dependent mechanical hyperalgesia. Pain 154:2216-2226.

Asante CO, Wallace VC, Dickenson AH (2009) Formalin-induced behavioural hypersensitivity and neuronal hyperexcitability are mediated by rapid protein synthesis at the spinal level. Mol Pain 5:27.

Asante CO, Wallace VC, Dickenson AH (2010) Mammalian Target of Rapamycin Signaling in the Spinal Cord Is Required for Neuronal Plasticity and Behavioral Hypersensitivity Associated With Neuropathy in the Rat. J Pain.

Asiedu MN, Tillu DV, Melemedjian OK, Shy A, Sanoja R, Bodell B, Ghosh S, Porreca F, Price TJ (2011) Spinal protein kinase M zeta underlies the maintenance mechanism of persistent nociceptive sensitization. The Journal of neuroscience : the official journal of the Society for Neuroscience 31:6646-6653.

Bogen O, Alessandri-Haber N, Chu C, Gear RW, Levine JD (2012) Generation of a pain memory in the primary afferent nociceptor triggered by PKCepsilon activation of CPEB. J Neurosci 32:2018-2026.

Boitano S, Flynn AN, Schulz SM, Hoffman J, Price TJ, Vagner J (2011) Potent agonists of the protease activated receptor 2 (PAR2). J Med Chem 54:1308-1313.

Breckenridge LJ, Wilson RJA, Connolly P, Curtis ASG, Dow JAT, Blackshaw SE, Wilkinson CDW (1995) Advantages of Using Microfabricated Extracellular Electrodes for in-Vitro Neuronal Recording. Journal of Neuroscience Research 42:266-276.

Bureau I, Shepherd GM, Svoboda K (2008) Circuit and plasticity defects in the developing somatosensory cortex of FMR1 knock-out mice. J Neurosci 28:5178-5188.

Carracedo A, Ma L, Teruya-Feldstein J, Rojo F, Salmena L, Alimonti A, Egia A, Sasaki AT, Thomas G, Kozma SC, Papa A, Nardella C, Cantley LC, Baselga J, Pandolfi PP (2008) Inhibition of mTORC1 leads to MAPK pathway activation through a PI3K-dependent feedback loop in human cancer. The Journal of Clinical Investigation 118:3065-3074.

Chaplan SR, Bach FW, Pogrel JW, Chung JM, Yaksh TL (1994) Quantitative assessment of tactile allodynia in the rat paw. J Neurosci Methods 53:55-63.

Codeluppi S, Svensson CI, Hefferan MP, Valencia F, Silldorff MD, Oshiro M, Marsala M, Pasquale EB (2009) The Rheb-mTOR pathway is upregulated in reactive astrocytes of the injured spinal cord. J Neurosci 29:1093-1104.
Costa-Mattioli M, Sossin WS, Klann E, Sonenberg N (2009) Translational control of long-lasting synaptic plasticity and memory. Neuron 61:10-26.
Coull JA, Boudreau D, Bachand K, Prescott SA, Nault F, Sik A, De Koninck P, De Koninck Y (2003) Trans-synaptic shift in anion gradient in spinal lamina I neurons as a mechanism of neuropathic pain. Nature 424:938-942.
Coull JA, Beggs S, Boudreau D, Boivin D, Tsuda M, Inoue K, Gravel C, Salter MW, De Koninck Y (2005) BDNF from microglia causes the shift in neuronal anion gradient underlying neuropathic pain. Nature 438:1017-1021.
Enright HA, Felix SH, Fischer NO, Mukerjee EV, Soscia D, McNerney M, Kulp K, Zhang J, Page G, Miller P, Ghetti A, Wheeler EK, Pannu S (2016) Long-term non-invasive interrogation of human dorsal root ganglion neuronal cultures on an integrated microfluidic multielectrode array platform. Analyst 141:5346-5357.
Ferrari LF, Araldi D, Levine JD (2015a) Distinct terminal and cell body mechanisms in the nociceptor mediate hyperalgesic priming. J Neurosci 35:6107-6116.
Ferrari LF, Bogen O, Chu C, Levine JD (2013) Peripheral Administration of Translation Inhibitors Reverses Increased Hyperalgesia in a Model of Chronic Pain in the Rat. J Pain.
Ferrari LF, Bogen O, Reichling DB, Levine JD (2015b) Accounting for the delay in the transition from acute to chronic pain: axonal and nuclear mechanisms. J Neurosci 35:495-507.
Flynn AN, Tillu DV, Asiedu MN, Hoffman J, Vagner J, Price TJ, Boitano S (2011) The protease-activated receptor-2-specific agonists 2-aminothiazol-4-yl-LIGRL-NH2 and 6-aminonicotinyl-LIGRL-NH2 stimulate multiple signaling pathways to induce physiological responses in vitro and in vivo. The Journal of biological chemistry 286:19076-19088.
Frega M, Pasquale V, Tedesco M, Marco M, Contestabile A, Nanni M, Bonzano L, Maura G, Chiappalone M (2012) Cortical cultures coupled to Micro-Electrode Arrays: A novel approach to perform in vitro excitotoxicity testing. Neurotoxicol Teratol 34:116-127.
Furic L, Rong L, Larsson O, Koumakpayi IH, Yoshida K, Brueschke A, Petroulakis E, Robichaud N, Pollak M, Gaboury LA, Pandolfi PP, Saad F, Sonenberg N (2010) eIF4E phosphorylation promotes tumorigenesis and is associated with prostate cancer progression. Proc Natl Acad Sci U S A 107:14134-14139.
Geranton SM, Jimenez-Diaz L, Torsney C, Tochiki KK, Stuart SA, Leith JL, Lumb BM, Hunt SP (2009) A rapamycin-sensitive signaling pathway is essential for the full expression of persistent pain states. J Neurosci 29:15017-15027.
Gkogkas CG, Khoutorsky A, Cao R, Jafarnejad SM, Prager-Khoutorsky M, Giannakas N, Kaminari A, Fragkouli A, Nader K, Price TJ, Konicek BW, Graff JR, Tzinia AK, Lacaille JC, Sonenberg N (2014) Pharmacogenetic inhibition of eIF4E-dependent Mmp9 mRNA translation reverses fragile X syndrome-like phenotypes. Cell Rep 9:1742-1755.
Gosselin RD, Varela C, Banisadr G, Mechighel P, Rostene W, Kitabgi P, Melik-Parsadaniantz S (2005) Constitutive expression of CCR2 chemokine receptor and inhibition by MCP-1/CCL2 of GABA-induced currents in spinal cord neurones. J Neurochem 95:1023-1034.
Grossman AW, Aldridge GM, Weiler IJ, Greenough WT (2006) Local protein synthesis and spine morphogenesis: Fragile X syndrome and beyond (vol 26, pg 7151, 2006). Journal of Neuroscience 26.
Hanson JE, Madison DV (2007) Presynaptic Fmr1 genotype influences the degree of synaptic connectivity in a mosaic mouse model of fragile X syndrome. Journal of Neuroscience 27:4014-4018.
Hargreaves K, Dubner R, Brown F, Flores C, Joris J (1988) A new and sensitive method for measuring thermal nociception in cutaneous hyperalgesia. Pain 32:77-88.

Herdy B et al. (2012) Translational control of the activation of transcription factor NF-kappaB and production of type I interferon by phosphorylation of the translation factor eIF4E. Nature immunology 13:543-550.
Hudmon A, Choi JS, Tyrrell L, Black JA, Rush AM, Waxman SG, Dib-Hajj SD (2008) Phosphorylation of sodium channel Na(v)1.8 by p38 mitogen-activated protein kinase increases current density in dorsal root ganglion neurons. J Neurosci 28:3190-3201.
Hylden JL, Wilcox GL (1980) Intrathecal morphine in mice: a new technique. Eur J Pharmacol 67:313-316.
Jimenez-Diaz L, Geranton SM, Passmore GM, Leith JL, Fisher AS, Berliocchi L, Sivasubramaniam AK, Sheasby A, Lumb BM, Hunt SP (2008) Local translation in primary afferent fibers regulates nociception. PLoS One 3:e1961.
Karim F, Wang CC, Gereau RWt (2001) Metabotropic glutamate receptor subtypes 1 and 5 are activators of extracellular signal-regulated kinase signaling required for inflammatory pain in mice. J Neurosci 21:3771-3779.
Kawasaki Y, Zhang L, Cheng JK, Ji RR (2008) Cytokine mechanisms of central sensitization: distinct and overlapping role of interleukin-1beta, interleukin-6, and tumor necrosis factor-alpha in regulating synaptic and neuronal activity in the superficial spinal cord. J Neurosci 28:5189-5194.
Khoutorsky A, Bonin RP, Sorge RE, Gkogkas CG, Pawlowski SA, Jafarnejad SM, Pitcher MH, Alain T, Perez-Sanchez J, Salter EW, Martin L, Ribeiro-da-Silva A, De Koninck Y, Cervero F, Mogil JS, Sonenberg N (2015) Translational control of nociception via 4E-binding protein 1. Elife 4.
Khoutorsky A, Sorge RE, Prager-Khoutorsky M, Pawlowski SA, Longo G, Jafarnejad SM, Tahmasebi S, Martin LJ, Pitcher MH, Gkogkas CG, Sharif-Naeini R, Ribeiro-da-Silva A, Bourque CW, Cervero F, Mogil JS, Sonenberg N (2016) eIF2alpha phosphorylation controls thermal nociception. Proc Natl Acad Sci U S A.
Knowlton WM, Palkar R, Lippoldt EK, McCoy DD, Baluch F, Chen J, McKemy DD (2013) A sensory-labeled line for cold: TRPM8-expressing sensory neurons define the cellular basis for cold, cold pain, and cooling-mediated analgesia. J Neurosci 33:2837-2848.
Langford DJ, Bailey AL, Chanda ML, Clarke SE, Drummond TE, Echols S, Glick S, Ingrao J, Klassen-Ross T, Lacroix-Fralish ML, Matsumiya L, Sorge RE, Sotocinal SG, Tabaka JM, Wong D, van den Maagdenberg AM, Ferrari MD, Craig KD, Mogil JS (2010) Coding of facial expressions of pain in the laboratory mouse. Nature methods 7:447-449.
Lee KY, Prescott SA (2015) Chloride dysregulation and inhibitory receptor blockade yield equivalent disinhibition of spinal neurons yet are differentially reversed by carbonic anhydrase blockade. Pain 156:2431-2437.
Martinez A, Sese M, Losa JH, Robichaud N, Sonenberg N, Aasen T, Ramon YCS (2015) Phosphorylation of eIF4E Confers Resistance to Cellular Stress and DNA-Damaging Agents through an Interaction with 4E-T: A Rationale for Novel Therapeutic Approaches. PLoS One 10:e0123352.
Matsuoka Y, Yokoyama M, Kobayashi H, Omori M, Itano Y, Morita K, Mori H, Nakanishi T (2007) Expression profiles of BDNF splice variants in cultured DRG neurons stimulated with NGF. Biochem Biophys Res Commun 362:682-688.
Melemedjian OK, Khoutorsky A (2015) Translational control of chronic pain. Prog Mol Biol Transl Sci 131:185-213.
Melemedjian OK, Asiedu MN, Tillu DV, Peebles KA, Yan J, Ertz N, Dussor GO, Price TJ (2010) IL-6- and NGF-Induced Rapid Control of Protein Synthesis and Nociceptive Plasticity via Convergent Signaling to the eIF4F Complex. J Neurosci 30:15113-15123.
Melemedjian OK, Tillu DV, Moy JK, Asiedu MN, Mandell EK, Ghosh S, Dussor G, Price TJ (2014) Local translation and retrograde axonal transport of CREB regulates IL-6-induced nociceptive plasticity. Mol Pain 10:45.
Melemedjian OK, Khoutorsky A, Sorge RE, Yan J, Asiedu MN, Valdez A, Ghosh S, Dussor G, Mogil JS, Sonenberg N, Price TJ (2013) mTORC1 inhibition induces pain via IRS-1-dependent feedback activation of ERK. Pain.

Melemedjian OK, Asiedu MN, Tillu DV, Sanoja R, Yan J, Lark A, Khoutorsky A, Johnson J, Peebles KA, Lepow T, Sonenberg N, Dussor G, Price TJ (2011) Targeting adenosine monophosphate-activated protein kinase (AMPK) in preclinical models reveals a potential mechanism for the treatment of neuropathic pain. Mol Pain 7:70.

Minett MS, Falk S, Santana-Varela S, Bogdanov YD, Nassar MA, Heegaard AM, Wood JN (2014) Pain without nociceptors? Nav1.7-independent pain mechanisms. Cell Rep 6:301-312.

Obara I, Geranton SM, Hunt SP (2012) Axonal protein synthesis: a potential target for pain relief? Curr Opin Pharmacol 12:42-48.

Obara I, Tochiki KK, Geranton SM, Carr FB, Lumb BM, Liu Q, Hunt SP (2011) Systemic inhibition of the mammalian target of rapamycin (mTOR) pathway reduces neuropathic pain in mice. Pain 152:2582-2595.

Pfeiffer BE, Huber KM (2007) Fragile X mental retardation protein induces synapse loss through acute postsynaptic translational regulation. Journal of Neuroscience 27:3120-3130.

Potter SM, DeMarse TB (2001) A new approach to neural cell culture for long-term studies. J Neurosci Methods 110:17-24.

Price TJ, Geranton SM (2009) Translating nociceptor sensitivity: the role of axonal protein synthesis in nociceptor physiology. Eur J Neurosci 29:2253-2263.

Price TJ, Inyang KE (2015) Commonalities between pain and memory mechanisms and their meaning for understanding chronic pain. Prog Mol Biol Transl Sci 131:409-434.

Price TJ, Prescott SA (2015) Inhibitory regulation of the pain gate and how its failure causes pathological pain. Pain 156:789-792.

Price TJ, Rashid MH, Millecamps M, Sanoja R, Entrena JM, Cervero F (2007) Decreased nociceptive sensitization in mice lacking the fragile X mental retardation protein: role of mGluR1/5 and mTOR. J Neurosci 27:13958-13967.

Pyronnet S, Imataka H, Gingras AC, Fukunaga R, Hunter T, Sonenberg N (1999) Human eukaryotic translation initiation factor 4G (eIF4G) recruits mnk1 to phosphorylate eIF4E. EMBO J 18:270-279.

Sonenberg N, Hinnebusch AG (2009) Regulation of translation initiation in eukaryotes: mechanisms and biological targets. Cell 136:731-745.

Thoreen CC, Chantranupong L, Keys HR, Wang T, Gray NS, Sabatini DM (2012) A unifying model for mTORC1-mediated regulation of mRNA translation. Nature 485:109-113.

Tillu DV, Hassler SN, Burgos-Vega CC, Quinn TL, Sorge RE, Dussor G, Boitano S, Vagner J, Price TJ (2015) Protease-activated receptor 2 activation is sufficient to induce the transition to a chronic pain state. Pain 156:859-867.

Ueda T, Watanabe-Fukunaga R, Fukuyama H, Nagata S, Fukunaga R (2004) Mnk2 and Mnk1 are essential for constitutive and inducible phosphorylation of eukaryotic initiation factor 4E but not for cell growth or development. Mol Cell Biol 24:6539-6549.

Waskiewicz AJ, Johnson JC, Penn B, Mahalingam M, Kimball SR, Cooper JA (1999) Phosphorylation of the cap-binding protein eukaryotic translation initiation factor 4E by protein kinase Mnk1 in vivo. Mol Cell Biol 19:1871-1880.

Wolfe AL et al. (2014) RNA G-quadruplexes cause eIF4A-dependent oncogene translation in cancer. Nature.

Yan J, Melemedjian OK, Price TJ, Dussor G (2012) Sensitization of dural afferents underlies migraine-related behavior following meningeal application of interleukin-6 (IL-6). Molecular Pain 8:6.

Zhuang ZY, Xu H, Clapham DE, Ji RR (2004) Phosphatidylinositol 3-kinase activates ERK in primary sensory neurons and mediates inflammatory heat hyperalgesia through TRPV1 sensitization. J Neurosci 24:8300-8309.

FIGURE LEGENDS

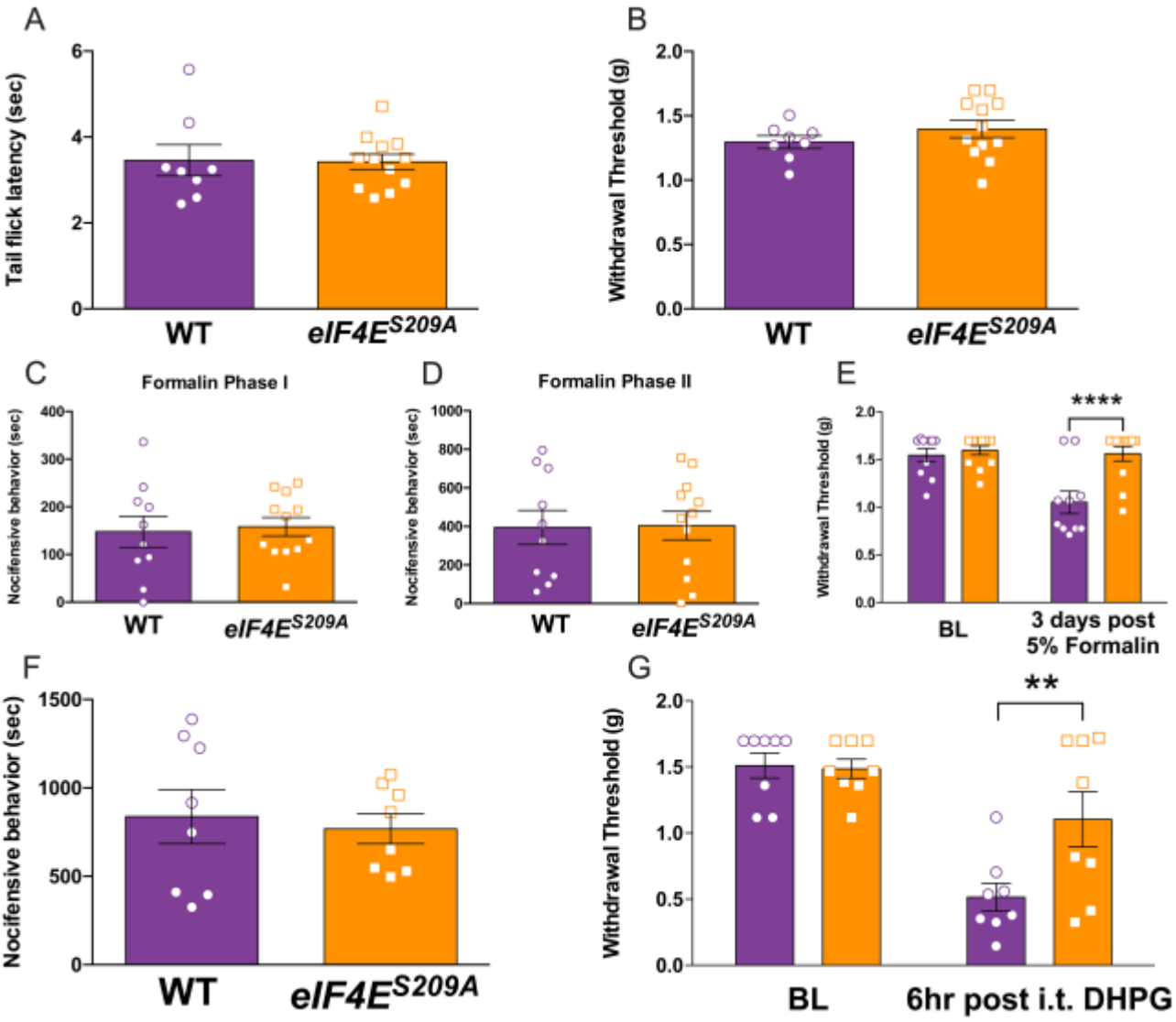

Figure 1. *eIF4E*^{S209A} mice have normal acute nociceptive responses but decreased mechanical hypersensitivity to formalin and a group I mGluR agonist. A) *eIF4E*^{S209A} and WT mice show no differences in tail-flick responses (55°C) *(n ≥ 6)* or **B)** baseline paw withdrawal thresholds *(n ≥ 6)*. **C, D)** First phase (0–10 min) and second phase (15–45 min) summed responses were not different between *eIF4E*^{S209A} and WT mice *(n ≥ 10)*. **E)** Three days post intraplantar (i.pl.) 5 % formalin injection *eIF4E*^{S209A} mice exhibited a significantly higher mechanical withdrawal threshold compared to WT mice *(n ≥ 10)*. **F, G)** The mGlu1/5 receptor agonist, DHPG (50 nmol), was injected intrathecally (i.t.) in both WT and *eIF4E*^{S209A} mice. Nocifensive behaviors summed during the 30 min after injection

were equal in both strains *(n = 8).* However, 6 hr post DHPG i.t. injection, WT mice exhibited mechanical hypersensitivity whereas eIF4E^{S209A} mice did not *(n = 8). **p<0.01; ****p<0.0001*

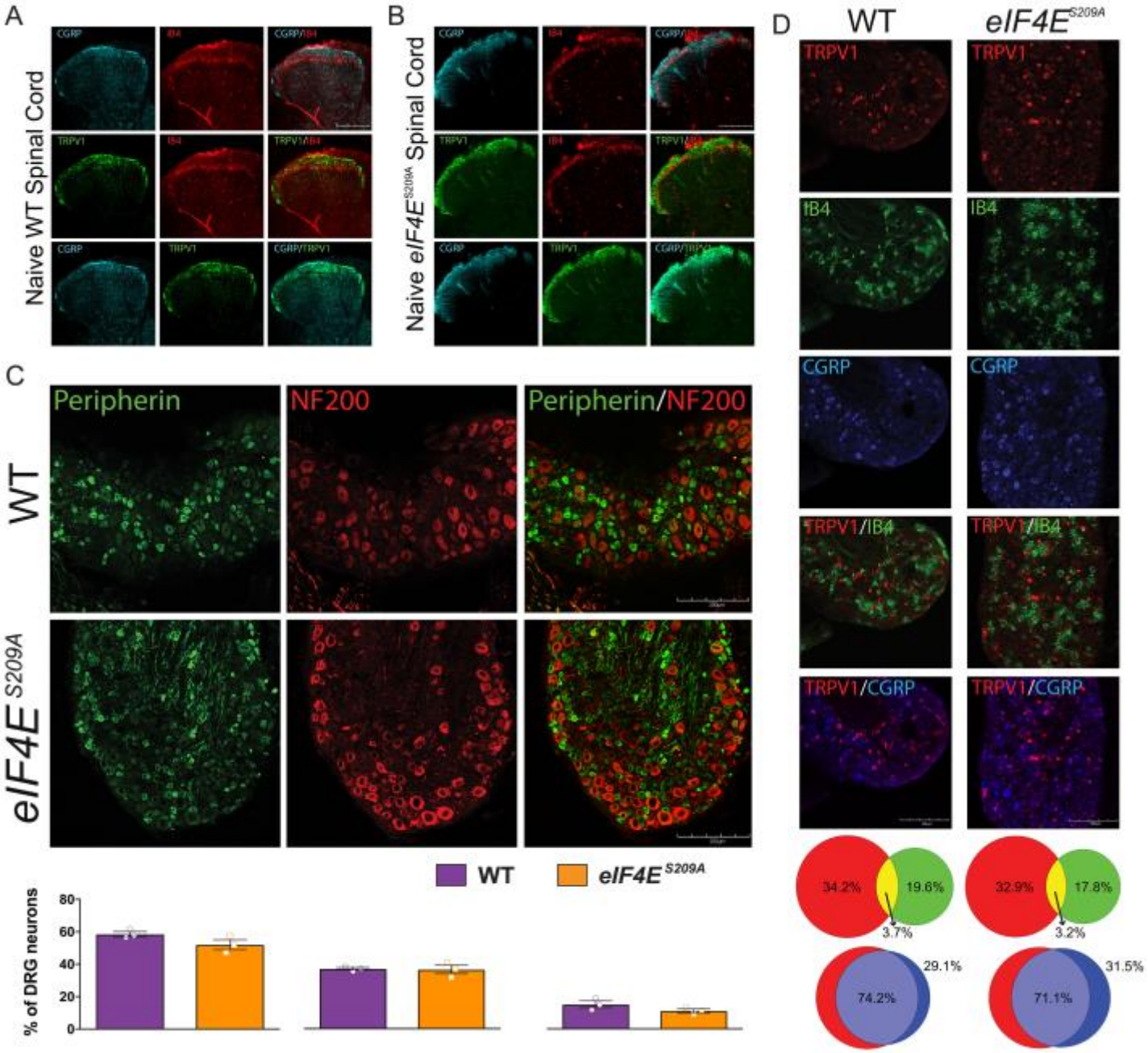

Figure 2. Normal development of nociceptive pathways in *eIF4E^{S209A}* mouse DRG and spinal cord. **A, B)** WT and *eIF4E^{S209A}* mouse spinal cords were immunostained with CGRP (cyan), TRPV1 (green), and IB$_4$ (red; *representative images from n = 3 mice).* **C)** Immunostaining for peripherin (green) and neurofilament 200 (NF200; red) in DRG from WT and *eIF4E^{S209A}* mice show no differences in the proportion of peripherin positive neurons per section *(n = 3),* the proportion of

NF200-positive neurons per section *(n = 3)* or in overlap between the two markers *(n = 3).* **D)** WT and *eIF4E*^{S209A} DRGs were stained for TRPV1 (red), IB_4 (green), and CGRP (blue), and the proportion of neurons expressing each marker was assessed *(TRPV1: WT mean = 34.3% ± 3.1% vs. eIF4E*^{S209A} *mean = 32.9% ± 1.3%; IB_4: WT mean = 19.6% ± 1.8% vs. eIF4E*^{S209A} *mean = 17.8% ± 2.0%; WT mean = CGRP: 29.1% ± 1.5% vs. eIF4E*^{S209A} *mean = 31.5% ± 2.0%)*. TRPV1 and IB_4 populations were segregated in both mouse strains *(TRPV1/IB_4 overlap: WT mean = 3.7% ± 0.1% vs. eIF4E*^{S209A} *mean = 3.2% ± 0.7%)* while TRPV1 and CGRP overlapped substantially *(TRPV1/CGRP overlap: WT mean = 74.2% ± 6.3% vs. eIF4E*^{S209A} *mean = 71.1% ± 2.3%)* as demonstrated in the proportional Venn diagrams. Scale bars represent 200 μm.

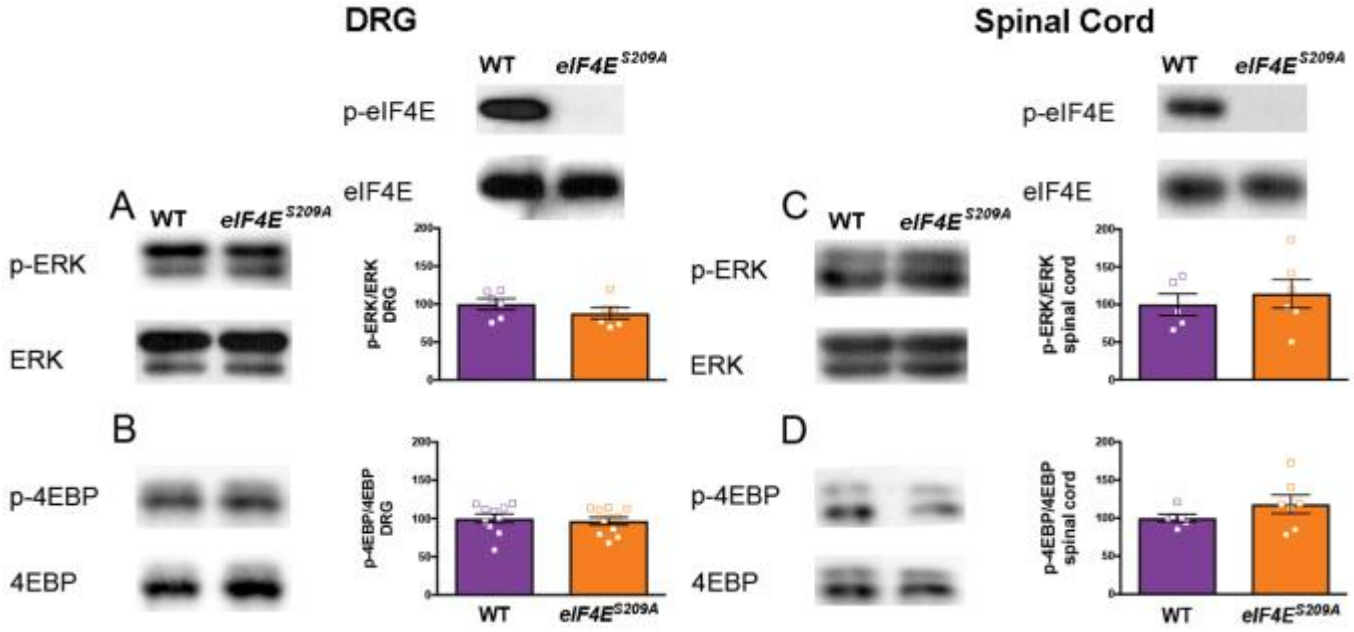

Figure 3. Normal ERK and 4E-BP phosphorylation in *eIF4E*^{S209A} mouse DRG and spinal cord.

A, B) *eIF4E*^{S209A} DRG shows equal levels of ERK and 4E-BP phosphorylation while eIF4E phosphorylation is completely absent compared to WT DRG using western blot analysis (n ≥ *6).* **C, D)** Additionally, spinal cord from *eIF4E*^{S209A} shows similar levels of p-ERK and p-4E-BP compared to WT spinal cord (n ≥ *5).*

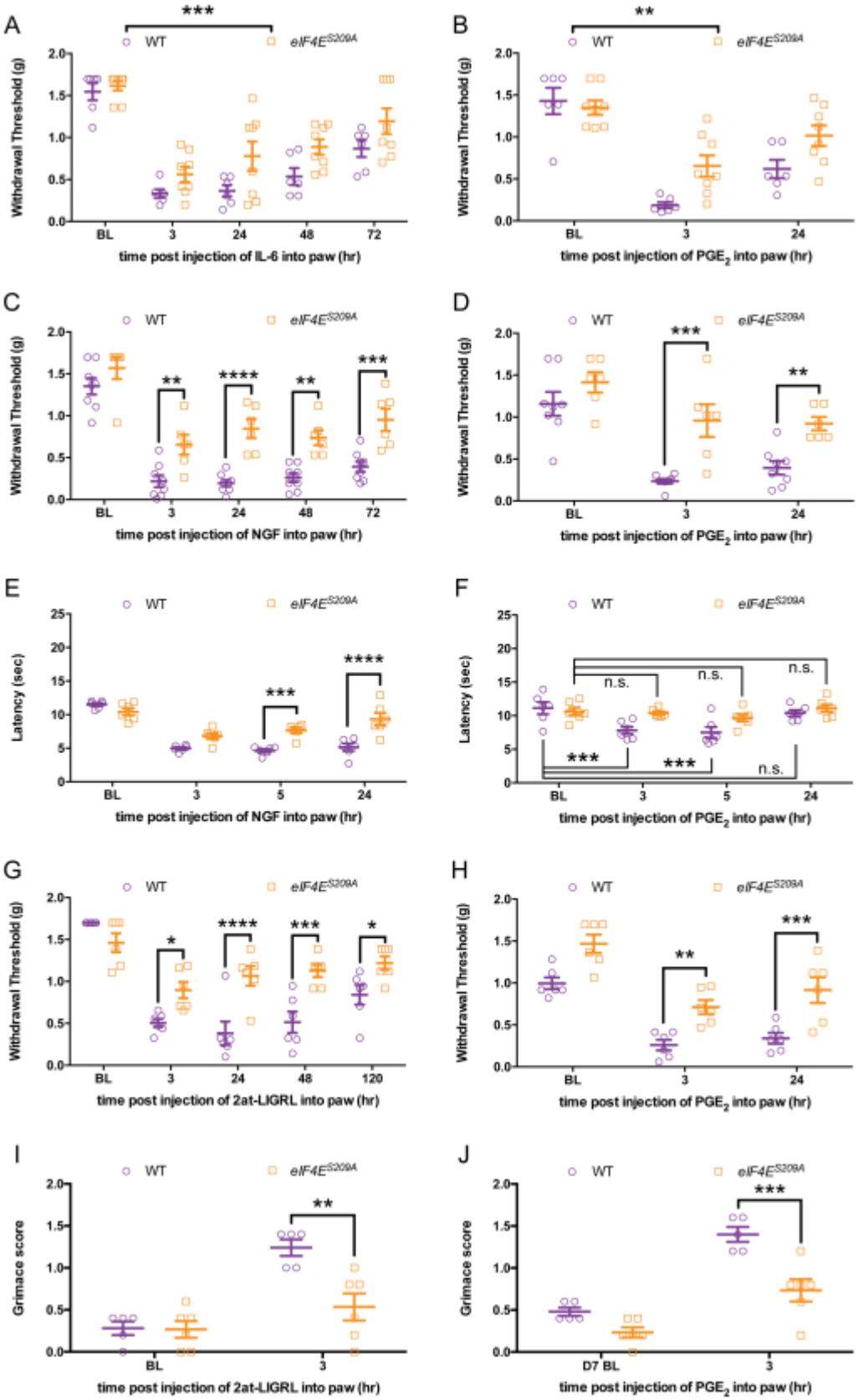

Figure 4. Mechanical and thermal hypersensitivity, facial grimacing, and the development of hyperalgesic priming are decreased in *eIF4E^{S209A}* mice. A) IL-6 (0.1 ng) was injected into the

hindpaw in both WT and *eIF4E*^{S209A} mice. Hindpaw mechanical thresholds were measured at 3, 24, 48, and 72 hr. *eIF4E*^{S209A} mice exhibited reduced mechanical hypersensitivity compared to WT mice and **(B)** a deficit in hyperalgesic priming *(n ≥ 6)*. **C)** *eIF4E*^{S209A} mice also demonstrated decreased mechanical and (**D,** *n = 6*) thermal hypersensitivity in response to i.pl. injection of 50 ng NGF *(n ≥ 6)* and ***(E, F)*** NGF-induced hyperalgesic priming. **G)** I.pl. injection of 20 ng 2at-LIGRL likewise induced decreased mechanical hypersensitivity in *eIF4E*^{S209A} mice and a decrease of hyperalgesic priming in response to IL-6 **(H,** *n ≥ 6,***)**, ***I)*** 2at-LIGRL induces facial grimacing in WT but not in eIF4E^{S209A} mice, ***(*J)** moreover, *eIF4E*^{S209A} mice fail to show facial grimacing after 2at-LIGRL priming when subsequently challenged with PGE_2 *(n ≥ 6). *p<0.05; **p<0.01; ***p<0.001 ****p<0.0001*

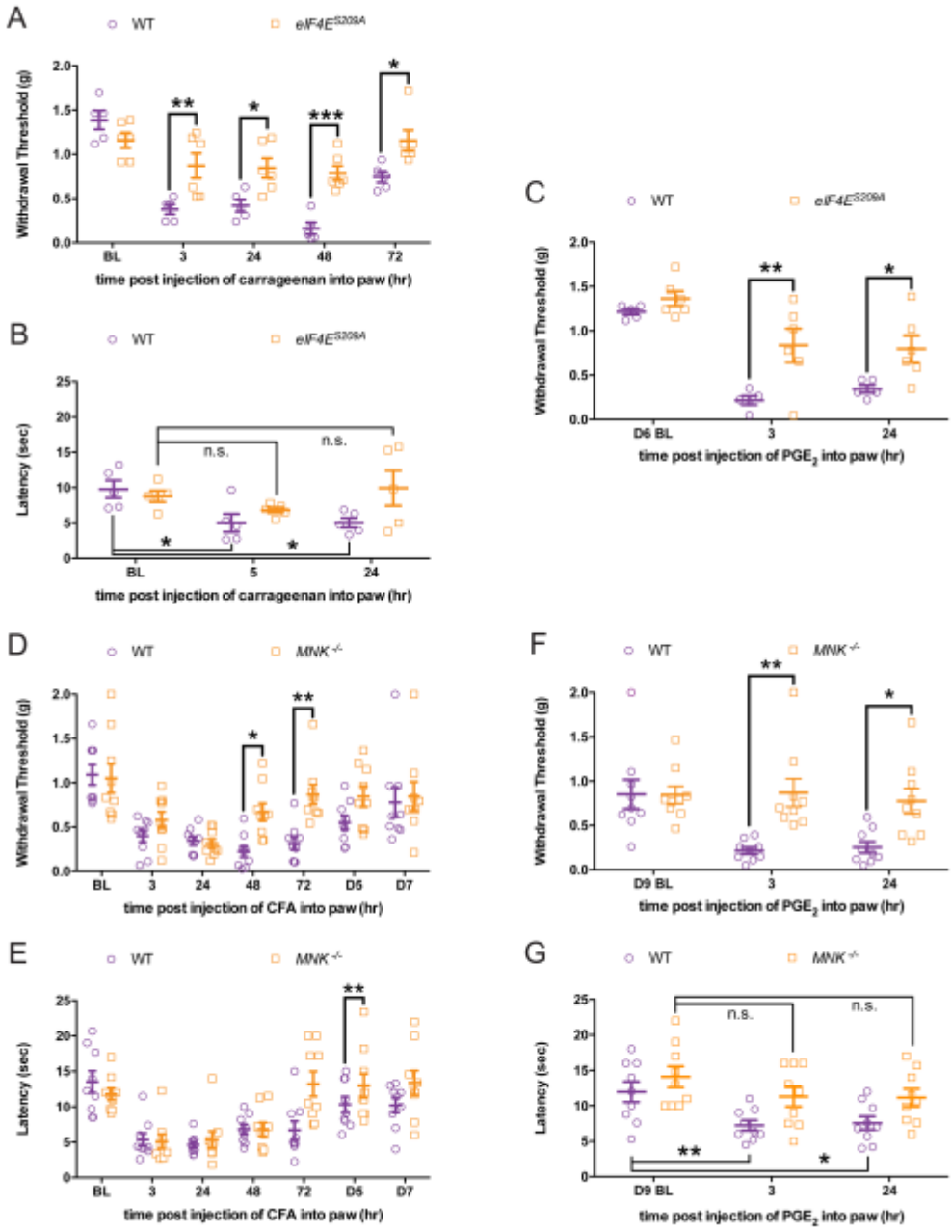

Figure 5. MNK1/2 – eIF4E signaling contributes to the development of mechanical and thermal hypersensitivity and hyperalgesic priming in response to inflammatory stimuli. A, B) Carrageenan (0.5% w/v) was injected into the hindpaw in both WT and *eIF4E*^{S209A} mice. Hindpaw mechanical and thermal thresholds show that *eIF4E*^{S209A} mice exhibited a blunted mechanical and thermal hypersensitivity compared to WT mice (*n* ≥ *5).* **C)** *eIF4E*^{S209A} mice developed reduced hyperalgesic priming when injected with PGE_2 (*n* ≥ *5).* **D, E)** *Mnk1/2*$^{-/-}$ mice injected i.pl. with CFA (0.5 mg/mL, 10µL) recover faster in both mechanical and thermal hypersensitivity compared to WT

mice (*n = 9).* **F, G)** *Mnk1/2*$^{-/-}$ mice show decreased mechanical and thermal response to PGE_2 after recovering from the initial hypersensitivity from CFA (*n = 9). *p<0.05; **p<0.01; ***p<0.001*

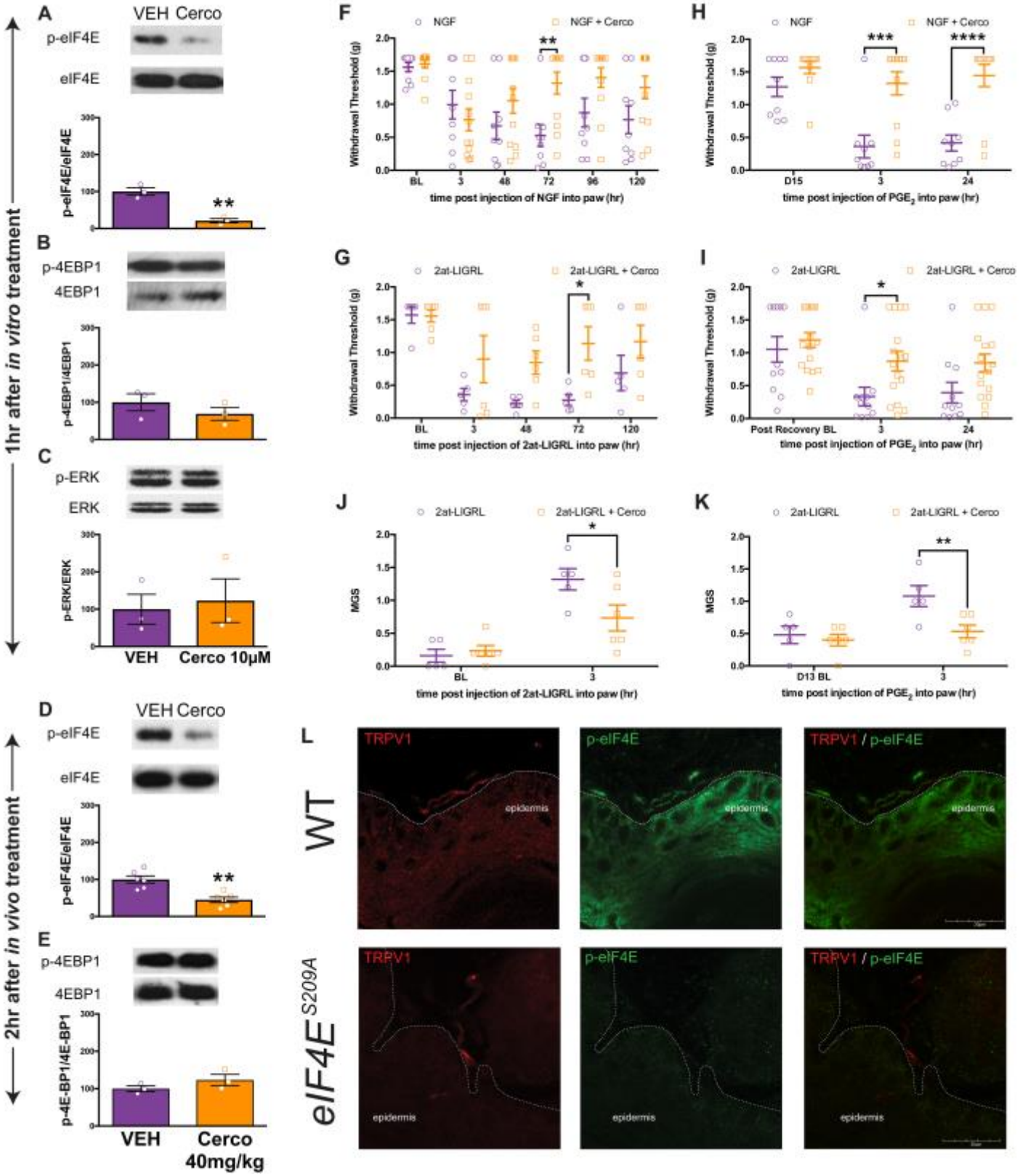

Figure 6. Local inhibition of MNK1/2 with cercosporamide reduces eIF4E phosphorylation, mechanical hypersensitivity, grimacing, and inhibits the development of hyperalgesic priming. **A)** One hr *in vitro* treatment of DRG neurons with cercosporamide (cerco, 10 μM) decreased eIF4E phosphorylation *(n = 3)* but did not influence 4E-BP1 phosphorylation *(***B***, n = 3)* or ERK phosphorylation *(***C**, *n = 3)*. **D)** Intraperitoneal injection of cercosporamide (40 mg/kg) results in a decreased eIF4E phosphorylation in DRGs *(n = 3)* but does not affect 4E-BP1 phosphorylation *(***E**, *n = 3).* **F, G)** Mechanical hypersensitivity induced by NGF (50 ng) or 2at-LIGRL (20 ng) was reduced by cercosporamide (10 μg, *n ≥ 9).* Similar to *eIF4E*^{S209A} mice, pharmacological inhibition of MNK1/2 using cercosporamide attenuated the development of hyperalgesic priming induced by NGF **(H)** and 2at-LIGRL **(I)** *(n ≥ 5).* **J)** Facial grimacing induced by i.pl. injection of 2at-LIGRL (20 ng) was also attenuated with local cercosporamide (10 μg) treatment as was facial grimacing with subsequent PGE_2 challenge *(***K**, n ≥ 5*).* **L)** Immunostaining of glabrous skin for TRPV1 (red) and p-eIF4E (green) revealed that eIF4E phosphorylation is present in TRPV1-positive fibers in WT, but absent in *eIF4E*^{S209A} mice. Scale bar represents 20 μm. **p<0.05; **p<0.01; ***p<0.001; ****p<0.0001*

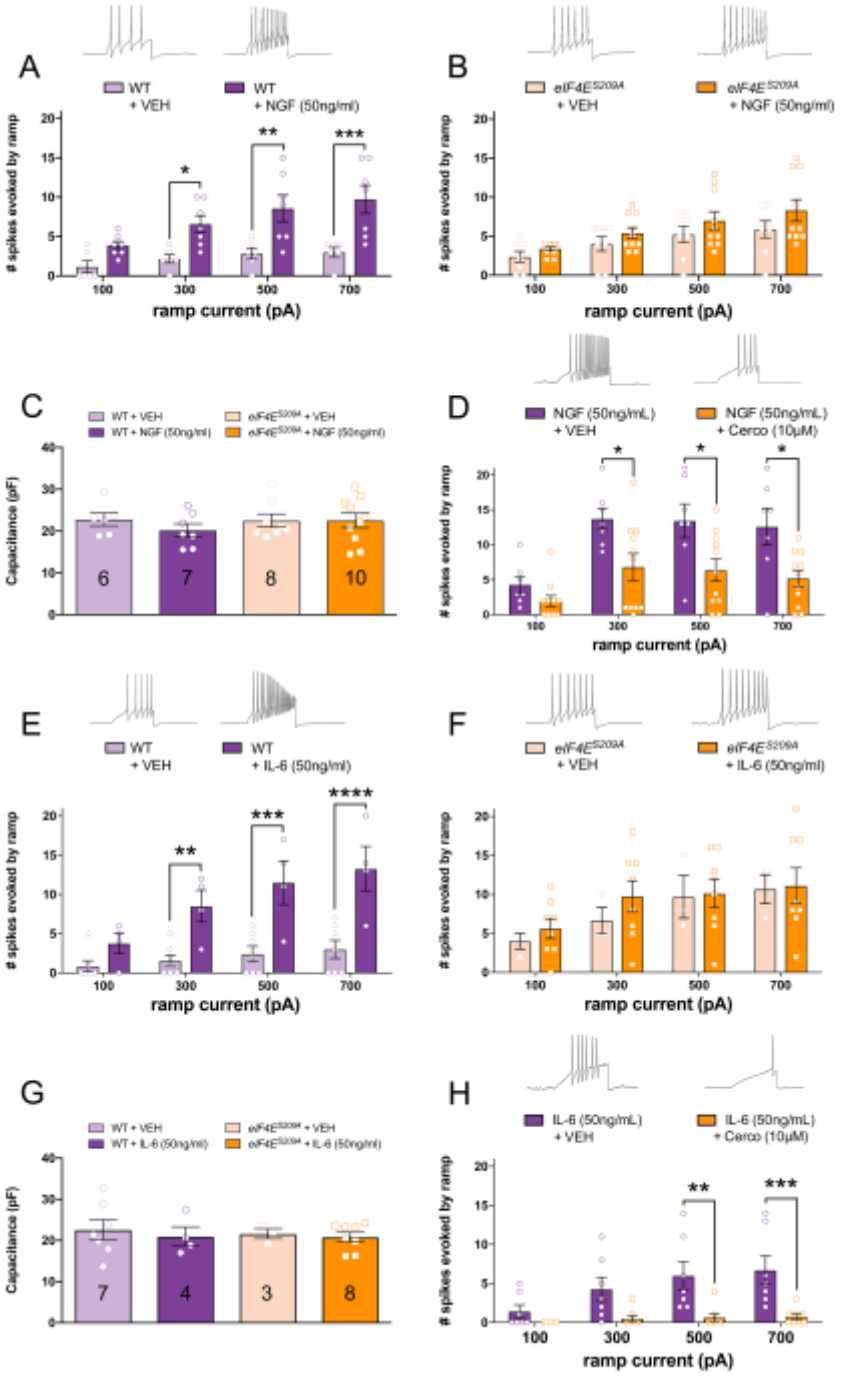

Figure 7. MNK1/2 - eIF4E signaling mediates NGF- and IL-6- induced changes in excitability in DRG neurons. A) WT DRG neurons were exposed to NGF or vehicle 18-24 hr prior to patch clamp recordings. Ramp current-evoked spiking demonstrates that NGF exposure increases the excitability of WT DRG neurons. ***B)*** *eIF4E*^{S209A} DRG neurons showed no difference in the number of spikes evoked by ramp currents between NGF and vehicle-treated DRG neurons. **C)** Membrane capacitance measures between WT and *eIF4E*^{S209A} DRG neurons show no difference in neuron size between

samples demonstrating that small diameter neurons were used for recordings. **D)** Pharmacological inhibition of MNK1/2 using cercosporamide (10 μM, *n* ≥ *9*) recapitulated the effect seen in *eIF4E*^{S209A} DRG neurons blocking NGF-induced hyperexcitability. **E*)*** IL-6 (50 ng/ml) exposure to WT DRG neurons for 1 hr caused an increase in excitability compared to vehicle but failed to do so in *eIF4E*^{S209A} DRG neurons **(F*)*. G)** Membrane capacitance between these samples was not different. N for each condition is shown in the appropriate bar. **H)** Cercosporamide blocked enhanced excitability induced by IL-6 in small diameter DRG neurons (50ng/mL) *(n ≥ 7)*. Traces shown in all panels are for the 700 pA stimulus. **p<0.05; **p<0.01; ***p<0.001*

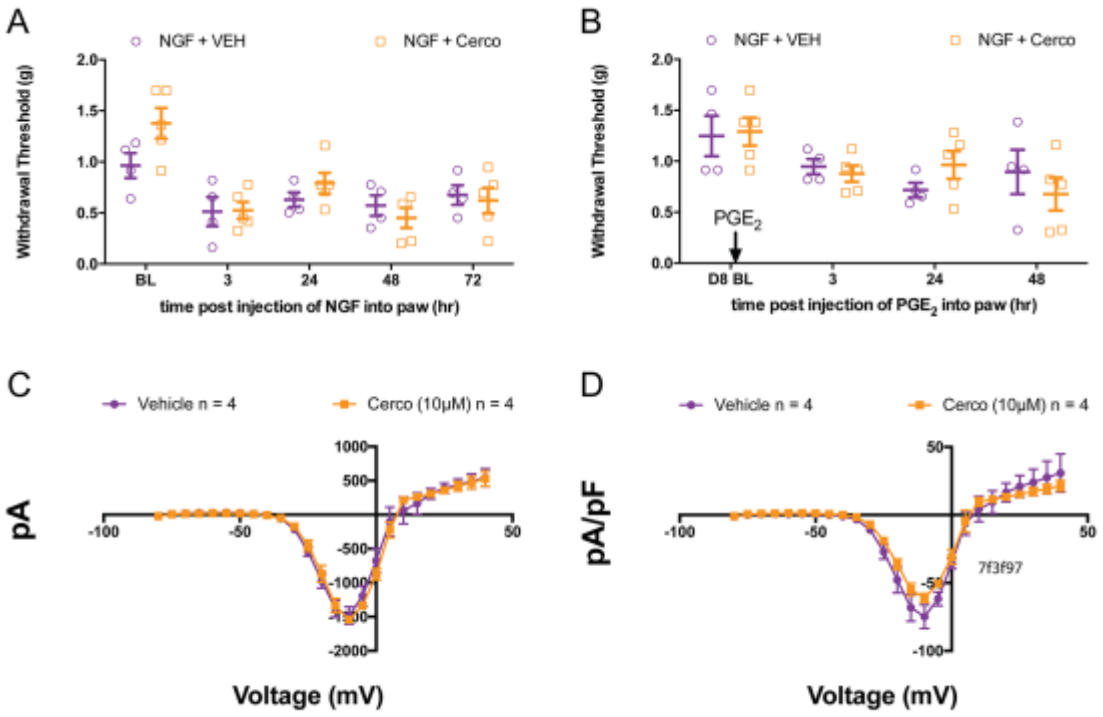

Figure 8. Cercosporamide has no additional effect in *eIF4E*^{S209A} mice and no acute effect on sodium current density. A) Mechanical hypersensitivity induced by NGF (50 ng) showed no difference between *eIF4E*^{S209A} mice that additionally received a hindpaw injection of cercosporamide (10 μg) and *eIF4E*^{S209A} mice that did not *(n ≥ 4, p > 0.05, two-way ANOVA)*. **B)** Subsequent injection of PGE_2 to precipitate priming also shows no difference between *eIF4E*^{S209A} mice that previously received cercosporamide and *eIF4E*^{S209A} mice that did not *(n ≥ 4, p > 0.05, two-way ANOVA)*. Sodium current **(C)** and sodium current density **(D)** were measured in WT DRG neurons with cercosporamide

(10 μM) perfused acutely over a 5-10 sec period *(n = 4, p > 0.05, two-way ANOVA)* indicating the cercosporamide does not block voltage-gated sodium channels at this concentration.

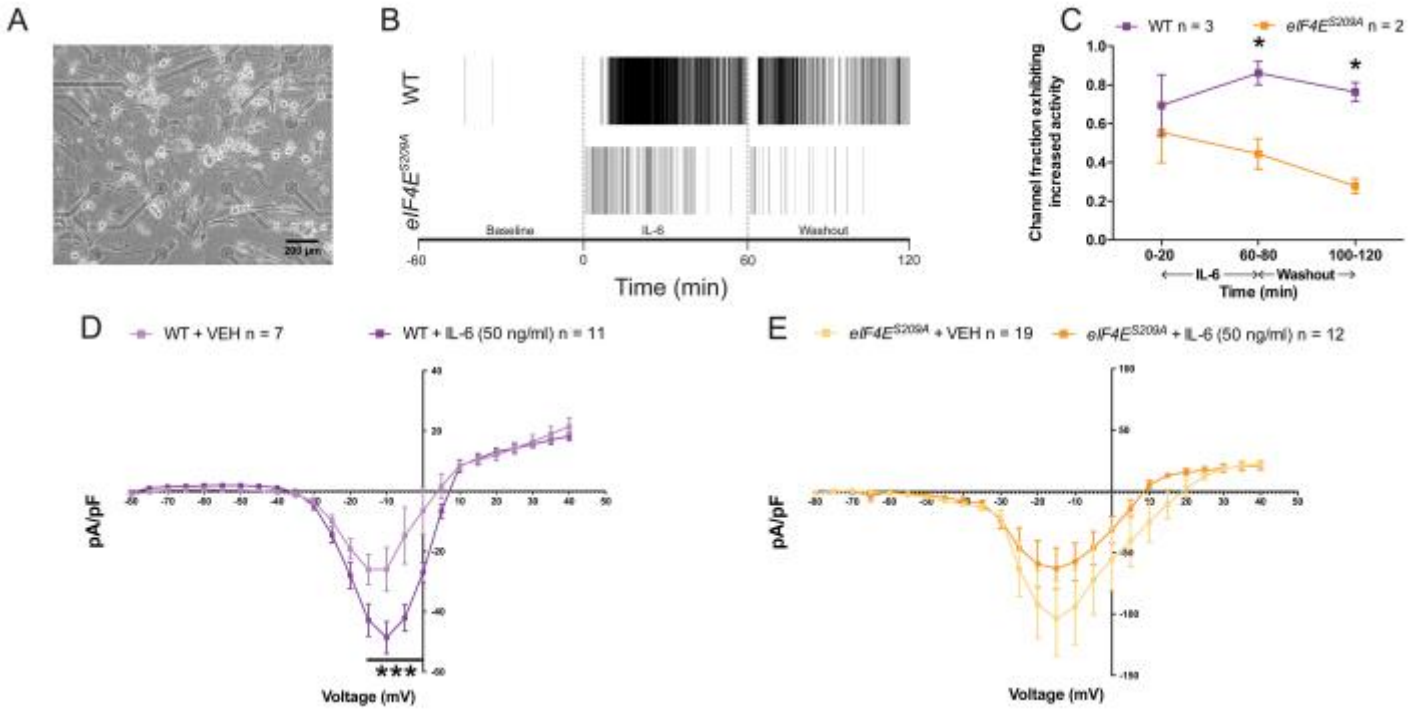

Figure 9. IL6-induced sustained spiking and increased voltage gated sodium current density is altered in *eIF4E^{S209A}* DRG neurons. A) Image of DRG neurons cultured on an MEA device. Scale bar represents 200μm. **B)** Raster plot showing electrical activity of WT and *eIF4E^{S209A}* DRG neuronal networks observed using MEAs during BL, IL-6 treatment, and 1 hr wash. **C)** IL-6 elicited increased spiking in WT DRG cultures during treatment that was sustained throughout the washout period and significantly greater than spiking observed in *eIF4E^{S209A}* DRG neurons. **D, E)** Sodium current density was increased after 1 hr after IL-6 exposure in WT DRG neurons, but was decreased in *eIF4E^{S209A}* DRG neurons (*WT: n ≥ 7, eIF4E^{S209A}: n ≥ 12). *p<0.05, ***p<0.001*

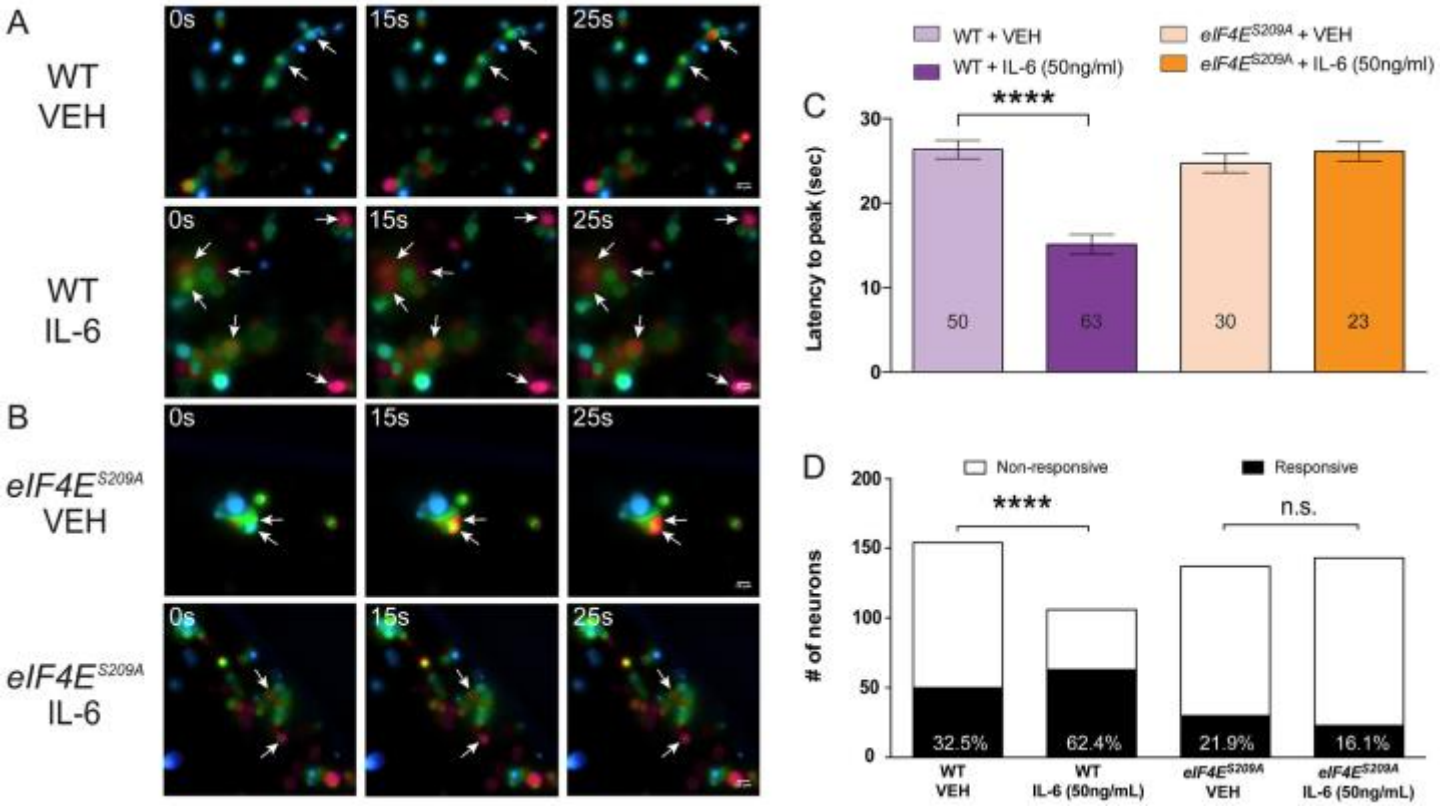

Figure 10. IL-6 treatment alters PGE_2 responsiveness in DRG neurons in an eIF4E phosphorylation-dependent fashion. WT and *eIF4E*^{S209A} DRG neurons were cultured and treated with VEH or IL-6 (50 ng/mL) for 1 hr. PGE_2 (1 nM) was perfused for 30 sec during which Ca^{2+} responses were measured **(A & B). C)** IL-6 treatment decreased the latency of PGE_2-evoked Ca^{2+} release in WT DRG neurons compared to vehicle-treated WT neurons *(n ≥ 50).* **D)** The proportion of neurons responding to PGE_2 was increased after IL-6 exposure in WT DRG neurons but was unchanged in *eIF4E*^{S209A} DRG neurons. Scale bar represents 20 µm. ****$p<0.0001$

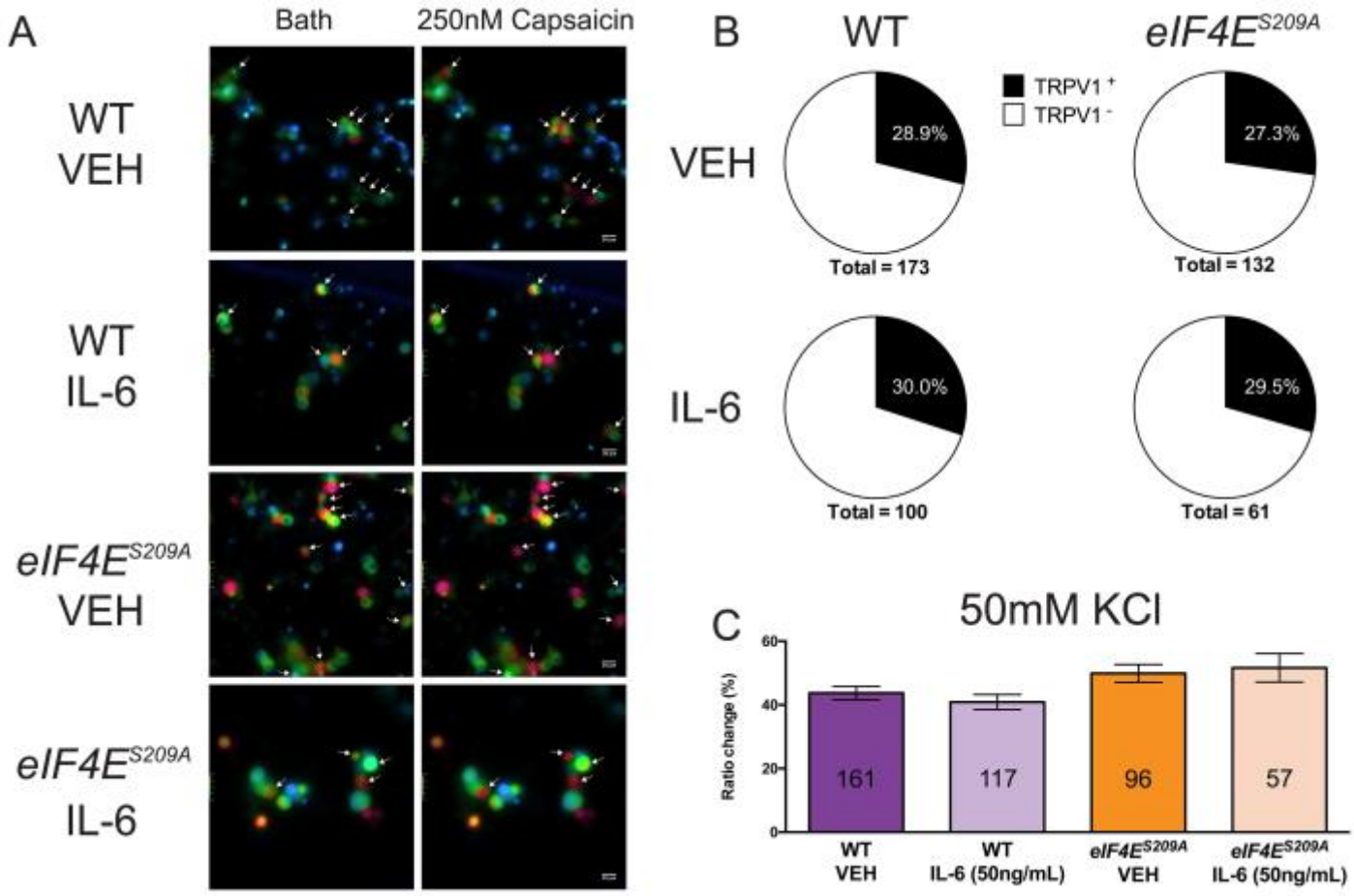

Figure 11. Normal Ca^{2+} signaling evoked by KCl and capsaicin in eIF4E^{S209A} DRG neurons. A) WT and *eIF4E^{S209A}* DRG neurons were imaged after 1 hr vehicle or IL-6 (50 ng) treatment during vehicle-containing bath solution and capsaicin (250 nM)-containing bath solution perfusions. **B)** The proportion of TRPV1-positive neurons were unchanged in WT and *eIF4E^{S209A}* DRG neurons treated with vehicle of IL-6. **C)** Moreover, Ca^{2+} signaling evoked by KCl (50 mM) was unchanged in all conditions *(n ≥ 57 neurons per condition, p>0.05, one-way ANOVA).* Scale bar represents 20 µm.

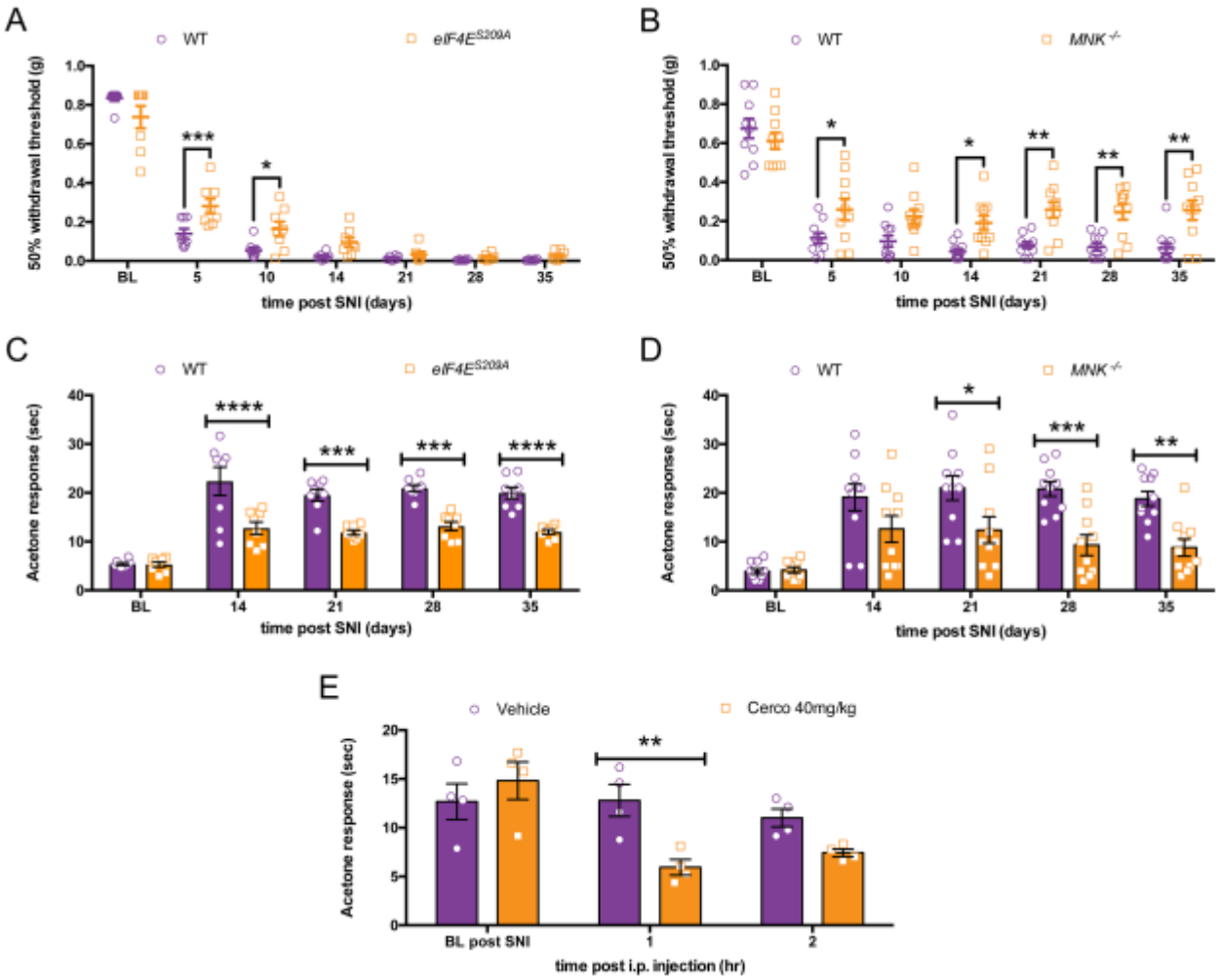

Figure 12. Decreased neuropathic pain in *eIF4E^{S209A}* mice and through MNK1/2 inhibition. A) Following SNI surgery *eIF4E^{S209A}* mice show reduced mechanical hypersensitivity that normalizes 14 days following surgery compared to WT mice *(n = 8).* **B)** *Mnk1/2$^{-/-}$* mice show blunted mechanical hypersensitivity lasting 35 days post SNI surgery *(n = 10).* **C)** Following SNI *eIF4E^{S209A}* mice have a decrease in cold hypersensitivity as measured in the acetone test compared to WT mice *(n = 8).* **D)** *Mnk1/2$^{-/-}$* mice show a sustained decrease in cold hypersensitivity after SNI compared to WT mice *(n = 10).* **E)** Following systemic administration of cercosporamide (40 mg/kg) for 3 days, WT mice show a transient decrease in cold hypersensitivity *(n = 4)*. *p<0.05; **p<0.01; ***p<0.001; ****p<0.0001.

TABLES

Table 1: List of antibodies used in this study.

Primary antibodies	Catalog number	Incubation	Secondary antibodies
eIF4E	phospho- 9741S phospho (IHC)- ab76256 total- 9742S	p- 1:500; p(IHC)- 1:1000; t- 1:1000; overnight @ 4 °C	Goat anti-rabbit (WB:1:10,000; IHC:1:1,000); 1 hr @ RT
4EBP1	phospho- 9459S total- 9452S	p- 1:500; t- 1:1000; overnight @ 4 °C	Goat anti-rabbit (1:10,000); 1 hr @ RT
ERK	phospho- 9101S total- 9102S	p- 1:3,000; t- 1:3,000; overnight @ 4 °C	Goat anti-rabbit (1:10,000); 1 hr @ RT
GAPDH	2118	1:10,000; overnight @ 4 °C	Goat anti-rabbit (1:10,000); 1 hr @ RT
Peripherin	SAB 4502419	1:500; overnight @ 4 °C	Alexa-fluor goat anti-rabbit 488 (1:1,000); 1 hr @ RT
Neurofilament 200	N0142	1:400; overnight @ 4 °C	Alexa-fluor goat anti-mouse 568 (1:1,000); 1 hr @ RT
Isolectin B_4- 568	I21412	Spinal cord- 1:1000; DRG- 1:400; overnight @ 4 °C	none
CGRP	T-4032	Spinal cord & DRG- 1:1000; overnight @ 4 °C	Alexa-fluor goat anti-rabbit 647 (1:2,000); 1 hr @ RT
TRPV1	GP14100	Spinal cord & DRG- 1:1000; Skin- 1:3,000; overnight @ 4 °C	Alexa-fluor goat anti-guinea pig 488 (1:2,000); 1 hr @ RT

Table 2: Sex of animals by genotype in behavioral experiments in this study.

Test	WT Males	WT Females	*eIF4E*^{S209A} Males	*eIF4E*^{S209A} Females
Tail Flick/ von Frey	4	4	7	5
Formalin	6	4	7	5
DHPG	5	3	4	4
IL-6	5	3	6	4
NGF	4	4	4	2
NGF thermal	-	6	-	6
2at-LIGRL (PAR_2)	4	2	4	2
Grimace [2at-LIGRL (PAR_2)]	4	1	-	6
Carrageenan	5	-	6	-
Carrageenan thermal	5	-	5	-
CFA ($MNK^{-/-}$)	4	5	4 (*$MNK^{-/-}$*)	5 (*$MNK^{-/-}$*)
Cercosporamide + NGF (in *eIF4E*^{S209A} mice)	-	-	4	7
SNI	4	4	6	2
SNI (in *$MNK^{-/-}$ mice)*	10	-	10 (*$MNK^{-/-}$*)	-
Cercosporamide (SNI)	4	4	-	-

Table 3: Different translation regulation pathways control different aspects of pain and pain amplification

Mutant mouse	Thermal	Mechanical	Thermal hyperalgesia	Mechanical hyperalgesia	Proposed mechanism
$eIF4E^{S209A}$	Normal	Normal	Decreased to inflammatory stimuli	Decreased to inflammatory stimuli	Decreased nociceptor plasticity
$MNK^{-/-}$	Normal	Normal	Decreased to inflammatory stimuli	Decreased to inflammatory stimuli and neuropathic	Decreased nociceptor plasticity
$Eif4ebp1^{-/-}$ (Khoutorsky et al., 2015)	Normal	Increased sensitivity	Not tested	Increased hypersensitivity to inflammatory stimuli	Decreased spinal neuroligin 1
$eIF2\alpha^{+/S51A}$(Khoutorsky et al., 2016)	Decreased sensitivity	Normal	Not tested	Decreased hypersensitivity to inflammatory stimuli	Decreased TRPV1 functional activity in DRG
Fmr1 KO (Price et al., 2007)	Normal	Normal	Not tested	Decreased hypersensitivity to inflammatory and neuropathic stimuli	Decreased spinal and peripheral mGluR1/5 & mTOR signaling